

Approximating Smiles: A Time Change Approach

Liexin Cheng, Xue Cheng

April 2024

Abstract

We introduce a novel method for approximating the shape of implied volatility smiles, applicable to widely-used semimartingale models, including jump-diffusion, rough volatility, and infinite activity models. First, we employ an Edgeworth expansion technique to approximate the at-the-money skew and curvature, establishing conditions that ensure the convergence of approximation errors. Subsequently, we explicitly determine the volatility skew and curvature within a time-change framework using moment-based formulas. Additionally, we derive the characteristics of volatility skew and curvature, elucidating their implications for model selection based on the approximations. The accuracy of our short-term approximation results is validated through numerical methods and empirical data. Finally, we apply the method to calibration problems for the guess of initial parameters.

Keywords: Implied volatility; Time change; Asymptotic approximation

Contents

1	Introduction	2
2	Time change Models and SVMs	4
2.1	Jump-diffusion Case	5
2.2	Rough Volatility Case	7
2.3	Infinite Activity Models	7
3	Approximation of Implied Volatility	8
3.1	A Model-free Characterization	8
3.2	Limiting Behavior and Examples	10
3.3	Approximations Under Time Change Framework	12

4	Approximations under Specific Models and Implication on Model Selection	13
4.1	Volatility Skew	14
4.2	Curvature	16
5	Numerical Results	18
5.1	Heston Model	19
5.2	Jump-diffusion Models	24
6	Empirical Application	27
6.1	Data Processing	27
6.2	Fitting the IVS	28
6.3	Calibration to the IVS	31
7	Conclusion	34
A	Proof of Theorem 1 and Proposition 1	39
B	Proof of Theorem 2	43
C	Proof of Theorem 3	46
D	Proof of Proposition 2 and Proposition 3	48
E	Proof of Proposition 4	50
F	Proof of Proposition 5	50
G	Proof of Corollary 2	52
H	Supplementart Graphs	53
H.1	2D plots of Term structure for Heston Model	53
H.2	Comparison of Two Approximations in Jump models	54

1 Introduction

The Black-Scholes implied volatility (IV) is a dimensionless metric that characterizes future volatility in an option market, given a specific strike price and maturity. It is customary to assess an option market by quoting its implied volatility.

Due to its dimensionless and interpretable nature, direct analysis of the volatility smile (or volatility surface, a collection of smiles across various maturities)

is more convenient. This study specifically examines several key of the implied volatility smile: at-the-money (ATM) skew, ATM curvature, and term structure.

In option markets the ATM skew typically shows a negative trend, resulting in a smile-shaped volatility curve that slopes downward. This non-constant volatility skew is effectively captured by traditional stochastic volatility models (SVMs) such as those by [Heston \(1993\)](#), [Hull and White \(1987\)](#), among others. Notably, the ATM skew tends to be more pronounced in short-term options, often posing challenges for continuous SVMs. [Carr and Wu \(2003\)](#) suggest incorporating jumps to account for these sharp skew dynamics, whereas [Gatheral et al. \(2018\)](#) and [Guyon \(2021\)](#) advocate rough volatility models for short-term IV behavior. Empirically, the ATM skew of IV typically decays at a power-law rate of ($O(\tau^{-\alpha})$) with ($\alpha \in (0.3, 0.5)$), particularly in the short term ([Gatheral et al. \(2018\)](#)).

The curvature of the IV smile dictates the rate of skew change and is therefore pivotal in shaping its overall form. This study demonstrates that curvature reflects market leverage levels within small maturities.

Selecting a model that aligns with empirical observations is crucial for market practitioners. How does the choice of model impact the form of the IV smile? What model features are necessary to reproduce desired characteristics? Extensive literature addresses these questions, focusing on SVM expansions and approximations of ATM skew and curvature. We limit our discussion to SVMs.

Various studies approximate IV smiles using the Edgeworth/Gram-Charlier expansion ([Jarrow and Rudd \(1982\)](#), [Corrado and Su \(1996\)](#), [Backus et al. \(2004\)](#), [Chateau et al. \(2017\)](#), [El Euch et al. \(2019\)](#)), adjusting higher-order moments beyond the Black-Scholes framework. ATM skew and curvature relate directly to the distributional skewness and kurtosis of asset log returns. [Bergomi and Guyon \(2012\)](#), [Guyon \(2021\)](#) extend IV smiles to second-order terms, incorporating volatility-of-volatility dynamics in continuous SVMs. [Alos et al. \(2007\)](#) and [Alos and León \(2017\)](#) employ Malliavin calculus to derive explicit short-term IV expressions. [Aït-Sahalia et al. \(2021\)](#) and [Medvedev and Scaillet \(2007\)](#) extend IV smiles across moneyness and maturity dimensions, while [Berestycki et al. \(2004\)](#) explore IV approximations using PDE methods.

This list is not exhaustive; further references include [Friz et al. \(2018\)](#), [Forde et al. \(2012\)](#), [Osajima \(2007\)](#), [Pagliarani and Pascucci \(2017\)](#), [Kristensen and Mele \(2011\)](#), [Xiu \(2014\)](#). Extreme cases also merit consideration; [Lee \(2004\)](#) examines volatility skew and curvature under extreme strikes, while [Forde and Jacquier \(2011\)](#) addresses long-term maturity scenarios.

Our study aims to approximate IV smiles comprehensively, considering expansions and model dependencies. Our contributions are novel in several respects.

First, we unify the approximation of volatility smiles across jump-diffusion, rough volatility, and time-changed Lévy models ([Carr and Wu \(2004\)](#)). This gen-

erality stems from expressing log returns as time-changed Lévy processes. Time change models are general in its distribution. In particular, [Monroe \(1978\)](#) establishes an equivalence in law between a semimartingale and a time changed Brownian motion.

Second, we derive explicit expressions for ATM skew and curvature using Edgeworth expansion and time-change methods, establishing their accuracy across a broad model class. We identify conditions under which these approximations hold true and validate them through numerical simulations.

Third, our approximations for ATM skew and curvature are intuitive and interpretable, incorporating model structures such as leverage, volatility of volatility, and jumps. These expressions elucidate the different impact of diffusion and jump components on both short-term and long-term IV smiles.

Finally, our approach innovates in smile approximation by representing general stochastic volatility models as time-change processes. We use Wald's equations in continuous time to express high-order volatility moments.

The paper is structured as follows: Section 2 introduces time-change models and their relationship with general SVMs. Section 3 details IV smile approximations and ATM skew/curvature. Section 4 analyzes ATM skew and curvature properties across different model types. Sections 5 and 6 present numerical and empirical experiments demonstrating our approximations' efficacy and practical applications. Section 7 concludes.

2 Time change Models and SVMs

In this section, we establish the relationship between time-changed Lévy models (TCLMs) and a class of general stochastic volatility models (GSVMs), including diffusion models, jump-diffusion models, rough volatility models, and infinite activity models. A Lévy process $(L(t))$ on a filtered probability space $(\Omega, \mathcal{F}, \{\mathcal{F}_t\}_{t \geq 0}, \mathbb{P})$ is a continuous-time process with independent and stationary increments, characterized by a characteristic function $(\phi_L(m; t) = e^{t\Psi_L(m)})$, where the characteristic exponent $(\Psi_L(m))$ is given by

$$\Psi_L(m) = i\alpha m - \frac{m^2}{2}\sigma^2 + \int_{\mathbb{R}} (e^{imx} - 1 - imx1_{|x| \leq 1}) \nu(dx),$$

with parameters $\alpha \in \mathbb{R}$, $\sigma \in \mathbb{R}^+$, and ν as a positive measure on \mathbb{R} such that $\nu(0) = 0$ and $\int_{\mathbb{R}} (|x|^2 \wedge 1) \nu(dx) < \infty$.

A time change $T = T_t, t \geq 0$ is a non-decreasing, continuous process where T_t is a stopping time with respect to $\{\mathcal{F}_t\}_{t \geq 0}$ for every $t \geq 0$. A time-changed Lévy process is of the form L_T .

Consider the financial asset price process characterized by a TCLM under a risk-neutral probability measure \mathbb{Q} :

$$S_t = S_0 e^{(r-\delta)t + X_t},$$

where r is the risk-free rate, δ is the dividend rate and X is modeled as L_T or its linear combination.

2.1 Jump-diffusion Case

Firstly, we demonstrate that a TCLM can represent a broad range of jump-diffusion GSVMs, such as the double exponential jump diffusion by [Kou \(2002\)](#), normal jump models by [Merton \(1976\)](#), the Hull-White model by [Hull and White \(1987\)](#), and affine jump diffusion models by [Duffie et al. \(2000\)](#). Under a risk-neutral probability, the log return process on time interval $[0, \tau]$ is described by:

$$\begin{aligned} dX_t &= \left(-\frac{v_t}{2} - \lambda_t \bar{\mu} \right) dt + \sqrt{v_t} dW_t + J^S dN_t, \\ dv_t &= \mu(v_t) dt + \gamma(v_t) dW_{2,t} + J^V dN_{2,t}, \end{aligned} \tag{1}$$

with nonnegative initial condition (X_0, v_0) . Here W, W_2 are standard Brownian motions, $dW_t dW_{2,t} = \rho dt$, N, N_2 are doubly stochastic Poisson processes with stochastic intensity λ_t , and jump sizes J^S, J^V are independent of X . The constant $\bar{\mu} = \mathbb{E}[\exp(J^S)] - 1$ is chosen to satisfy the martingale condition.

Assumption 1 $\mu : \mathbb{R}_+ \rightarrow \mathbb{R}$ and $\gamma : \mathbb{R}_+ \rightarrow \mathbb{R}$ are continuous functions with linear growth:

$$|\mu(x)| + |\gamma(x)| \leq a|x| + b, \quad \forall x > 0$$

for some $a, b > 0$, and are such that v is almost surely positive on $[0, \tau]$.

If, in addition, $\mu(\cdot)$ and $\gamma(\cdot)$ satisfy Assumption 1, then there exists a unique weak solution $(X, v) = (X_t, v_t)_{t \leq \tau}$ to the SDE system (1). Furthermore, the log return X can be expressed as the sum of time-changed Lévy processes $\tilde{B}_U + \tilde{L}_V$, having the same law. Specifically:

$$\begin{aligned} U_t &= \int_0^t v_s ds, \quad V_t = \int_0^t \lambda_s ds, \\ \hat{U}_t &= \inf\{s : U_s > t\}, \\ B_t &= \int_0^{\hat{U}_t} \sqrt{v_s} dW_s, \quad L_t = \sum_{i=1}^{\tilde{N}_t} J^S, \end{aligned}$$

where \tilde{N} is a Poisson process with unit jump intensity independent of W, W_2 . The definition applies analogously to B_2 and L_2 , and the new Lévy processes and variance processes are:

$$\begin{aligned} d\tilde{B}_t &= -\frac{1}{2}dt + dB_t, \\ d\tilde{L}_t &= -\Psi_L(-i)dt + dL_t, \\ dv_t &= \mu(v_t)dt + \frac{\gamma(v_t)}{\sqrt{v_t}}dB_{2,U_t} + J^V dL_{2,V_t}. \end{aligned}$$

The leverage effect is inherited by B and B_2 as $[B, B_2]_t = \rho \int_0^{\hat{U}_t} v_s ds = \rho U_{\hat{U}_t} = \rho t$. It can be shown that $X \stackrel{\text{law}}{=} \tilde{B}_U + \tilde{L}_V$. For multi-factor jump-diffusion models with multiple variance processes, the corresponding TCLMs incorporate multiple time changes as $X_t = \sum_{i=1}^n \tilde{L}_{i,T_{i,t}}$, where $\{\tilde{L}_i, 1 \leq i \leq n\}$ are independent Lévy processes and $\{T_i, 1 \leq i \leq n\}$ are time changes.

Example 1 In the double exponential stochastic jump-diffusion model by [Huang et al. \(2014\)](#), the price process follows:

$$\begin{cases} dS_t/S_t = (r - \delta - \lambda_t \bar{\mu})dt + \sqrt{v_t}dW_{1,t} + (e^J - 1) dN_t, \\ dv_t = \kappa_v (\theta_v - v_t) dt + \varepsilon_v \sqrt{v_t}dW_{2,t}, \\ d\lambda_t = \kappa_\lambda (\theta_\lambda - \lambda_t) dt + \varepsilon_\lambda \sqrt{\lambda_t}dW_{3,t}, \end{cases}$$

where J follows an asymmetric double exponential distribution and N is a doubly stochastic Poisson process with stochastic intensity λ_t . This model can be transformed into a TCLM, where the log return X_t is described by:

$$dX_t = \left(-\frac{v_t}{2} - \lambda_t \bar{\mu}\right)dt + \sqrt{v_t}dW_{1,t} + JdN_t.$$

Let $U_t = \int_0^t v_s ds$, $V_t = \int_0^t \lambda_s ds$ and define B, B_2, B_3, L accordingly. We have

$$\begin{aligned} d\tilde{B}_t &= -\frac{1}{2}dt + dB_t, \\ d\tilde{L}_t &= -\Psi_L(-i)dt + dL_t, \\ dv_t &= \kappa_v (\theta_v - v_t) dt + \varepsilon_v dB_{2,U_t}, \\ d\lambda_t &= \kappa_\lambda (\theta_\lambda - \lambda_t) dt + \varepsilon_\lambda dB_{3,V_t}, \end{aligned}$$

and $X \stackrel{\text{law}}{=} \tilde{B}_U + \tilde{L}_V$.

2.2 Rough Volatility Case

We consider a large family of rough volatility models, including rough Bergomi models by [Bayer et al. \(2016\)](#), rough Heston models by [El Euch and Rosenbaum \(2019\)](#), and a class of rough volatility models considered in [Abi Jaber and El Euch \(2019b\)](#). We consider a family of rough volatility models on time interval $[0, \tau]$ as follows:

$$\begin{aligned} dX_t &= -\frac{v_t}{2}dt + \sqrt{Y_t}dW_t, \\ Y_t &= g(v_t), \\ v_t &= v_0 + \int_0^t K(t-u)\mu(v_u)du + \int_0^t (t-u)^{\alpha-1}\gamma(v_u)dW_{2,u}, \end{aligned} \tag{2}$$

with initial condition (S_0, v_0) . Here g is a continuous mapping from \mathbb{R} to \mathbb{R}_+ , $\alpha \in (\frac{1}{2}, 1)$ is the roughness parameter, $dWdW_2 = \rho dt$.

Assumption 2 *There exists $\eta > 0$ and $C > 0$ such that for any $h > 0$,*

$$\int_0^h |K(s)|^2 ds + \int_0^{\tau-h} |K(h+s) - K(s)|^2 ds \leq Ch^\eta$$

If Assumption 1 and 2 are met for $\mu(\cdot)$, $\gamma(\cdot)$ and $K(\cdot)$, then it is shown ([Abi Jaber and El Euch \(2019a\)](#), Theorem A.1) that the SDE system (2) admits a continuous weak solution $(X, Y) = (X_t, Y_t)_{t \leq \tau}$. In this case, the log return takes the time-change form $X \stackrel{\text{law}}{=} \tilde{B}_T$, where

$$\begin{aligned} T_t &= \int_0^t g(Y_u)du, \quad \hat{T}_t = \inf\{s : T_s \geq t\}, \\ B_t &= \int_0^{\hat{T}_t} \sqrt{g(Y_u)}dW_u, \quad B_{2,t} = \int_0^{\hat{T}_t} \sqrt{g(Y_u)}dW_{2,u}, \\ d\tilde{B}_t &= -\frac{1}{2}dt + dB_t, \\ v_t &= v_0 + \int_0^t \mu(v_u, u)du + \int_0^t (t-u)^{\alpha-1} \frac{\gamma(v_u)}{\sqrt{g(v_u)}} dB_{2,T_u}. \end{aligned}$$

In this work, we consider the case when g is the identity function, i.e. $v \equiv Y$, for simplicity. Nevertheless, the results can be easily extended for g smooth enough.

2.3 Infinite Activity Models

In this family of models, the Lévy process is given by

$$\tilde{L}_t = B_{V_t} + \theta V_t,$$

where V is a Lévy subordinator independent of Brownian motion B . V is usually of infinite activity. The time change here is the calendar time $T_t \equiv t$. There are several common choices of the subordinator, see [Geman \(2002\)](#), [Carr et al. \(2002\)](#), [Madan and Yor \(2008\)](#) for details.

3 Approximation of Implied Volatility

3.1 A Model-free Characterization

In a model-free framework, the density of log returns at maturity can be decomposed using the Edgeworth expansion. Assuming the current time is $t = 0$ and the time to maturity is τ , this expansion approximates the distribution of X_τ by its cumulants. We assume that all moments of X_τ exist. Given that implied volatility depends solely on moneyness and not further on the risk-free rate or dividend yield (see Appendix [A](#)), we set $r = \delta = 0$ without loss of generality.

Furthermore, we define:

s : standard deviation of X_τ ,

γ_1 : skewness of X_τ ,

γ_2 : excess kurtosis of X_τ ,

κ_n : the n -th cumulant of $\frac{X_\tau - E[X_\tau]}{s}$,

k : log-moneyness of an option, $\log(K/S_0)$.

Theorem 1 *For small variance s^2 , the call price $C(K, \tau)$ can be approximated as follows:*

$$C(K, \tau) = S_0 \Phi(d) - K \Phi(d - s) + S_0 \varphi(d) s \left[\frac{\gamma_1}{3!} \frac{k}{s} + \frac{\gamma_2}{4!} \left(\frac{k^2}{s^2} + 2k - 1 \right) + \frac{10\gamma_1^2}{6!} \left(\frac{k^4}{s^4} + \frac{3k^3}{s^2} - \frac{6k^2}{s^2} - 9k + 3 \right) \right] + \epsilon,$$

where ϵ represents the error resulting from higher-order moments of X_τ , $\Phi(\cdot)$ and $\varphi(\cdot)$ are the distribution and density functions of the standard normal distribution, respectively, and $d = d(s)$ is defined by:

$$d = \frac{-k + s^2/2}{s}.$$

Remark 1 Similar results are reported in [Chateau et al. \(2017\)](#), [Backus et al. \(2004\)](#), [Corrado and Su \(1996\)](#), [Jarrow and Rudd \(1982\)](#). These works commonly employ the Gram-Charlier expansion up to the fourth moment. However, this truncation may introduce non-negligible errors, even for continuous GSVMS, as will be illustrated through numerical examples in [Section 5](#).

Corollary 1 For small s , the option implied volatility $v(k, \tau)$ is approximated up to a linear expansion as a quadratic function of moneyness:

$$v(k, \tau) = \frac{s}{\sqrt{\tau}} \left[1 + \frac{\gamma_1}{6s}k + \left(\frac{\gamma_2 - 2\gamma_1^2}{24s^2} \right)k^2 \right] + \epsilon_v, \quad (3)$$

where ϵ_v accounts for truncation errors from Edgeworth expansion and residual errors from Taylor expansion.

Remark 2 As shown in [Appendix A](#), formula (3) works fine for continuous models. But for jump models, the high-order cumulants are non-negligible at short maturity, and we present here an improved approximation:

$$v(k, \tau) = \frac{s}{\sqrt{\tau}} \left[\left(1 + \frac{\gamma_1^2 - \gamma_2}{24} \right) + \left(\frac{\gamma_1}{6s} + \frac{\gamma_2}{12} - \frac{\gamma_1^2}{8} \right)k + \left(\frac{\gamma_2 - 2\gamma_1^2}{24s^2} \right)k^2 + \frac{\gamma_1^2}{24s^2}k^3 + \frac{\gamma_1^2}{72s^4}k^4 \right] + \epsilon_v. \quad (4)$$

As a result of formula (3), we have the approximation for ATM skew

$$\psi(\tau) := \left. \frac{\partial v}{\partial k} \right|_{k=0} \approx \frac{\gamma_1}{6\sqrt{\tau}} \quad (5)$$

and ATM curvature

$$\text{Cur}(\tau) := \left. \frac{\partial^2 v}{\partial k^2} \right|_{k=0} \approx \frac{\gamma_2 - 2\gamma_1^2}{12s\sqrt{\tau}}. \quad (6)$$

The approximation indicates that the ATM skew is proportional to the skewness of log return γ_1 , and that the ATM curvature is proportional to the excess kurtosis of log return when the standard deviation remains constant.

Remark 3 When τ is moderately small, the low-order Edgeworth series is typically a good approximation of the original distribution with a small truncation error, see [Backus et al. \(2004\)](#) for example. But as $\tau \rightarrow 0$, the error ϵ_v may explode for certain models, e.g. jump-diffusion models and infinite activity models.

3.2 Limiting Behavior and Examples

In some cases, we are concerned with the limiting behavior of ATM skew and ATM curvature. Does the approximation error necessarily converge to zero as $\tau \rightarrow 0$? Do the approximations in (5) or (6) become accurate in the limit? To answer these questions, we first propose the following conditions:

Condition 1: The log return X is stochastically continuous: for any $\varepsilon > 0$ and $t \geq 0$, it holds that

$$\lim_{h \rightarrow 0} \mathbb{P}(|X_{t+h} - X_t| > \varepsilon) = 0.$$

Condition 2: There exists an $M > 0$ such that $|\frac{k}{s}| < M$ for all $\tau > 0$.

Condition 3: The cumulants of the normalized log return satisfy

$$\kappa_3 = o(1), \quad \kappa_4 = O(\kappa_3), \quad \kappa_n = o(\kappa_4), \quad n \geq 5, \quad \text{as } \tau \rightarrow 0.$$

Condition 1 is easily met for Lévy-type models. Condition 2 is typical for ATM approximations. Condition 3 is a mild restriction on the distribution of log returns, which many models can satisfy, as shown in the examples and Theorem 2 below.

Proposition 1 *Under condition 1-3, $\epsilon_v \rightarrow 0$ as $\tau \rightarrow 0$, and the approximations (5) and (6) are accurate in the sense that*

$$\psi(\tau) \sim \frac{\gamma_1}{6\sqrt{\tau}}, \quad \text{Cur}(\tau) \sim \frac{\gamma_2 - 2\gamma_1^2}{12s\sqrt{\tau}}, \quad \tau \rightarrow 0.$$

Example 2 (Deterministic Volatility) *Suppose the log return has deterministic volatility:*

$$X_t = B_{T_t} - \frac{1}{2}T_t,$$

where T is deterministic. A typical model of this type is Black-Scholes. X_τ follows a normal distribution and its cumulants $\kappa_n = 0$ for $n \geq 3$. Thus, condition 3 holds.

Example 3 (Heston Model)

$$\begin{aligned} dX_t &= -\frac{v_t}{2}dt + \sqrt{v_t}dW_t \\ dv_t &= \kappa(\theta - v_t)dt + \eta\sqrt{v_t}dZ_t, \end{aligned}$$

where $dW_t dZ_t = \rho dt$ and $\rho \neq 0$. The moment generating function of X_τ is

$$E[e^{uX_\tau}] = \exp(A(\tau, u) + B(\tau, u)v_0)$$

where (A, B) is the solution to the ODE system

$$\begin{aligned}\frac{\partial A(t, u)}{\partial t} &= \kappa \theta B(t, u), \\ A(0, u) &= 0, \\ \frac{\partial B(t, u)}{\partial t} &= \frac{u^2 - u}{2} - (\kappa - \rho u \eta) B(t, u) + \frac{\eta^2}{2} B(t, u)^2, \\ B(0, u) &= 0.\end{aligned}$$

The m -th cumulant $\kappa_m(X_\tau)$ is the coefficient of u^m in the Taylor expansion of

$$\ln E[e^{uX_\tau}] = A(\tau, u) + B(\tau, u)v_0$$

w.r.t. u . The form of ODE system guarantees that $A(t, u)$ and $B(t, u)$ are differentiable with respect to t of any order. By Taylor's expansion at $t = 0$:

$$\begin{aligned}A(t, u) &= \sum_{n=1}^{\infty} \frac{\partial^n A(0, u)}{\partial t^n} \frac{t^n}{n!}, \\ B(t, u) &= \sum_{n=1}^{\infty} \frac{\partial^n B(0, u)}{\partial t^n} \frac{t^n}{n!}.\end{aligned}$$

If u^m first appears in $A^{(n)}(0, u) := \frac{\partial^n A(0, u)}{\partial t^n}$ or $B^{(n)}(0, u) := \frac{\partial^n B(0, u)}{\partial t^n}$, then $\kappa_m(X_\tau) = O(\tau^n)$. Thus we are concerned with the largest order of u in the derivatives. By iterative arguments, we have

$$B^{(n)}(0, u) = (\rho u \sigma - \kappa) B^{(n-1)}(0, u) + \frac{\sigma^2}{2} \sum_{\substack{s+r=n-1, \\ s \geq 1, r \geq 1}} C_{sr} B^{(s)}(0, u) B^{(r)}(0, u). \quad (7)$$

When $n = 1$, $B'(0, u)$ has the largest order u^2 . Suppose that $B^{(q)}(0, u)$ has the highest-order term u^{q+1} for $1 \leq q \leq n-1$, then $B^{(n)}(0, u)$ has the highest-order term u^{n+1} by (7). The same argument applies to $A^{(n)}(0, u)$, and we find that the cumulants of log return $\kappa_n(X_\tau) = O(\tau^{n-1})$ for $n \geq 2$. After normalization, the cumulants have the order $\frac{n}{2} - 1$:

$$\kappa_n = O(\tau^{n-1}/\tau^{\frac{n}{2}}) = O(\tau^{\frac{n}{2}-1}) = o(\tau), \quad n \geq 2.$$

Thus, Condition 3 is met.

However, not every model satisfies Condition 3. The following infinite activity model is an extreme case.

Example 4 Assume the log return is of the form

$$X_t = B_{V_t} + \theta V_t,$$

where V is a Lévy subordinator independent of B . The moment generating function of X_τ is

$$E[e^{uX_\tau}] = e^{\Psi_V(\frac{-iu^2}{2} - iu\theta)\tau},$$

where $\Psi_V(\cdot)$ is the characteristic component of V . From the expression, we obtain $\kappa_n(X_\tau) = O(\tau)$. Then for such subordinated Brownian models, the n -th cumulant of the normalized log return has the order $1 - \frac{n}{2}$:

$$\kappa_n = O(\tau^{1-\frac{n}{2}}),$$

which violates condition 3 and explodes for $n > 2$.

A general result for the limiting behavior is summarized in the following theorem.

Theorem 2 The continuous GSVMs considered in section 2 satisfy condition 1-3. Thus, the approximations (5) and (6) for GSVMs become exact as $\tau \rightarrow 0$.

For the proof, see Appendix B.

In El Euch et al. (2019), it's also shown that the approximations (5) and (6) are exact for continuous SVMs and rough SVMs under mild regularity conditions. However, our conditions are easier to verify.

3.3 Approximations Under Time Change Framework

In this section, we compute the more explicit form of ATM skew and curvature under the framework of TCLMs $X = \tilde{L}_T$. Here, $\tilde{L}_t = L_t + \bar{\mu}t$ with $\bar{\mu} = \ln Ee^{L_1}$ and L having zero mean. For instance, when L is a standard Brownian motion, $\bar{\mu} = -\frac{1}{2}$. In the following, we denote by $T = T_\tau$ for simplicity when there's no confusion.

According to the continuous Wald's equations (Theorem 3, Hall (1970)), we have

$$\begin{aligned}\mu_2 &:= E(L_T)^2 = \sigma^2 ET, \\ \mu_3 &:= E(L_T)^3 = 3\sigma^2 E(TL_T) + \kappa_3^L ET, \\ \mu_4 &:= E(L_T)^4 = 6\sigma^2 E(TL_T^2) + 4\kappa_3^L E(TL_T) + \kappa_4^L ET - 3\sigma^4 ET^2,\end{aligned}\tag{8}$$

where $\kappa_i^L := \kappa_i(L_1)$.

For example, when L is a standard Brownian motion, $\sigma^2 = 1$, $\kappa_3^L = \kappa_4^L = 0$ and $EW_T^3 = 3ETW_T$, $EW_T^4 = 6ETW_T^2 - 3ET^2$. By combining equation (5), (6) and equation (8), we obtain the following expressions for volatility skew and curvature:

Theorem 3 *The ATM skew is approximated by*

$$\psi(\tau) \approx \frac{\text{Cov}(T, L_T)}{2\sigma\sqrt{\tau}(ET)^{\frac{3}{2}}} + \frac{\bar{\mu} \text{Cov}(T, L_T^2)}{2\sigma^3\sqrt{\tau}(ET)^{\frac{3}{2}}} + \frac{\gamma_1^L}{6\sqrt{\tau}ET}, \quad (9)$$

and the ATM curvature is approximated by

$$\begin{aligned} \text{Cur}(\tau) \approx & \frac{\text{Cov}(T, L_T^2) - 2\bar{\mu}ET \text{Cov}(T, L_T)}{2\sigma^3(ET)^{\frac{5}{2}}\sqrt{\tau}} + \frac{2\bar{\mu} \text{Cov}(T, L_T^3) + 3\bar{\mu}^2 E[\tilde{T}^2 L_T^2]}{6\sigma^5(ET)^{\frac{5}{2}}\sqrt{\tau}} \\ & - \frac{V(T)}{4\sigma\sqrt{\tau}(ET)^{\frac{5}{2}}} + \frac{\gamma_1^L ET L_T}{3\sigma^2(ET)^{\frac{5}{2}}\sqrt{\tau}} + \frac{\gamma_2^L}{12\sigma(ET)^{\frac{3}{2}}\sqrt{\tau}} \\ & - \frac{1}{6\sqrt{\tau}ET} \left(\frac{3 \text{Cov}(T, L_T)}{\sigma(ET)^{\frac{3}{2}}} + \frac{3\bar{\mu} \text{Cov}(T, L_T^2)}{\sigma^3(ET)^{\frac{3}{2}}} + \frac{\gamma_1^L}{\sqrt{ET}} \right)^2, \end{aligned} \quad (10)$$

where $\tilde{T} = T - ET$, γ_1^L is the skewness of L_1 and γ_2^L is the excess kurtosis of L_1 .

For the proof, see Appendix C.

The ATM skew is decomposed as a sum of the impacts from covariance and jump skewness. And the ATM curvature is decomposed into a sum of impacts from covariance, price jumps and their coefficients.

4 Approximations under Specific Models and Implication on Model Selection

In this section, we conduct an in-depth analysis of the properties of the approximated at-the-money (ATM) skew and ATM curvature as presented in Theorem 3 within specific models. We also derive the limiting expressions as $\tau \rightarrow 0$ for certain models. Our focus is on a specific class of time-changed Lévy models (TCLMs), which we refer to as generalized jump-diffusion models.

In this section, we analyze the properties of the approximated ATM skew and ATM curvature in Theorem 3 within specific models. We also derive the limiting expressions as $\tau \rightarrow 0$ for certain models. Our focus is on a specific class of TCLMs, which we refer to as generalized jump-diffusion models (GJDMs).

Definition 1 *The log return X is said to follow a **generalized jump-diffusion model** if $X = \tilde{L}_T$ with $T = \int_0^\cdot v_s ds$ and*

$$\begin{aligned} d\tilde{L}_t &= \bar{\mu}dt + dL_t, \\ dv_t &= \mu(v_t)dt + \gamma(v_t)dL_{2,T_t}, \end{aligned}$$

where function $\mu(\cdot)$ and $\gamma(\cdot)$ satisfy Assumption 1, L and L_2 are correlated zero-mean Lévy processes with

$$L_t = \rho_t L_{2,t} + \sqrt{1 - \rho_t^2} L_{3,t},$$

where $L_{3,t}$ is independent of $L_{2,t}$ and ρ_t is a deterministic process with $\lim_{t \rightarrow 0} \rho_t = \rho$.

Both jump-diffusion SVMs and infinite activity models can be characterized by a GJDM or its linear combination. Next, we further analyze the ATM skew and ATM curvature based on GJDMs.

4.1 Volatility Skew

Proposition 2 Consider a GJDM with $\gamma_1^L \neq 0$. The components of ATM skew (9) exhibit the following orders:

$$\frac{\text{Cov}(T, L_T)}{2\sigma\sqrt{\tau}(ET)^{\frac{3}{2}}} = \rho O(1), \quad \frac{\bar{\mu} \text{Cov}(T, L_T^2)}{2\sigma^3\sqrt{\tau}(ET)^{\frac{3}{2}}} = \rho^2 O(1), \quad \frac{\gamma_1^L}{6\sqrt{\tau}ET} = O(\tau^{-1}).$$

The proof of this proposition can be found in Appendix D.

Remark 4 The impact of covariance, represented by $\text{Cov}(T, L_T)$ and $\text{Cov}(T, L_T^2)$, is of order $O(1)$ as $\tau \rightarrow 0$. This implies that the covariance part of the ATM skew converges to a constant. However, the impact of skewness of base Lévy κ_3^L decays at a rate of τ^{-1} . Therefore, the ATM skew explodes as $\tau \rightarrow 0$ for GJDMs with skewed jumps.

From the proposition, it follows that the decay rate of the volatility skew is heterogeneous. The portion of the volatility skew induced by leverage and vol-of-vol converges for short maturities, hence it is persistent. In contrast, the portion induced by the skewness of the base jump process decays at a faster rate of $O(\tau^{-1})$. As a result, Consequently, models with jumps are expected to be flexible in calibrating to the entire IVS term structure.

Furthermore, in the absence of leverage, $\psi(\tau) \approx \frac{\gamma_1^L}{6\sqrt{\tau}ET}$, and the ATM skew solely arises from jump skewness.

As a special case, consider a continuous GSVM where the activity rate v follows a homogeneous diffusion process:

$$dv_t = \mu(v_t)dt + \gamma(v_t)dZ_t, \quad t \in [0, \tau], \quad (11)$$

with $dW_t dZ_t = \rho dt$ and $\mu(\cdot)$, $\gamma(\cdot)$ satisfying Assumption 1. In this case, the ATM skew takes a much simpler approximation.

Proposition 3 *For continuous GSVMs where v is a diffusion process in (11), the volatility skew has the approximation*

$$\psi(\tau) \approx \frac{\rho C^{xv}}{2\sqrt{\tau}(ET)^{\frac{3}{2}}}, \quad (12)$$

where

$$C^{xv} = E \left[\int_0^\tau (\tau - t) \sqrt{v_t} \gamma(v_t) dt \right] \quad (13)$$

represents the impact of vol-of-vol. Furthermore, the ATM skew takes the limit form

$$\lim_{\tau \rightarrow 0+} \psi(\tau) = \frac{\rho \gamma(v_0)}{4v_0}.$$

This result aligns with findings in Guyon (2021).

For instance, if we consider the Heston model where $\gamma(v_t) = \eta \sqrt{v_t}$, we obtain

$$\lim_{\tau \rightarrow 0+} \psi(\tau) = \frac{\rho \eta}{4\sqrt{v_0}}.$$

Moreover, this result can be extended to rough volatility models.

Proposition 4 *For a continuous GSVM with rough volatility given by*

$$v_t = v_0 + \int_0^t K(t-u) \mu(v_u) du + \int_0^t (t-u)^{\alpha-1} \gamma(v_u) dZ_u,$$

where the setup aligns with equation (2), the volatility skew approximation for short maturities takes the form

$$\psi(\tau) \approx \frac{\rho C^{xv}(\alpha)}{2\alpha\sqrt{\tau}(ET)^{\frac{3}{2}}},$$

where

$$C^{xv}(\alpha) = E \left[\int_0^\tau (\tau - t)^\alpha \gamma(v_t) \sqrt{v_t} dt \right].$$

In the limit, we have

$$\lim_{\tau \rightarrow 0+} \tau^{1-\alpha} \psi(\tau) = \frac{\rho \gamma(v_0)}{2\alpha(\alpha+1)\sqrt{v_0}}.$$

The proof for this proposition is provided in Appendix E.

Example 5 (rough Heston) Consider a rough Heston model ([El Euch and Rosenbaum \(2019\)](#))

$$\begin{aligned}\frac{dS_t}{S_t} &= \sqrt{v_t} dW_t, \\ v_t &= v_0 + \frac{1}{\Gamma(\alpha)} \int_0^t (t-s)^{\alpha-1} \kappa (\theta - v_s) ds + \frac{1}{\Gamma(\alpha)} \int_0^t (t-s)^{\alpha-1} \kappa \nu \sqrt{v_s} dZ_s, \\ dW_t dZ_t &= \rho dt,\end{aligned}$$

where $\alpha \in (\frac{1}{2}, 1)$, and κ, ν, θ are positive parameters. From [Proposition 4](#), we have

$$C^{xv}(\alpha) = \kappa \nu E \left[\int_0^\tau (\tau-t)^\alpha v_t dt \right].$$

We obtain

$$\lim_{\tau \rightarrow 0+} \tau^{1-\alpha} \psi(\tau) = \frac{\rho \kappa \nu}{D_\alpha \sqrt{v_0}},$$

where

$$D_\alpha = \frac{1}{2\Gamma(\alpha)\alpha(\alpha+1)}.$$

Although time-changed Brownian motion models can fit the volatility skew well by adding leverage and vol-of-vol structure, they often fit poorly to the entire volatility surface, as observed in [Gatheral et al. \(2018\)](#). Empirical studies show that the volatility skew explodes as $\tau \rightarrow 0$. This indicates that the return process has jump components or a rough volatility structure, as discussed in [Carr and Wu \(2003\)](#), [Bayer et al. \(2016\)](#) and [Gatheral et al. \(2018\)](#). The results in this paper are consistent with these findings. As shown in the equation (9), the effect of skewness γ_1^L explodes as $\tau \rightarrow 0$ for jump models and the effect of covariance explodes in proportion to $\tau^{H-\frac{1}{2}}$ for rough volatility models with $H < \frac{1}{2}$.

4.2 Curvature

Based on the expression of ATM curvature in [Theorem 3](#), we further analyze the properties of curvature and its relationship with model components.

Proposition 5 Consider a GJDM with $\gamma_1^L \neq 0$ and $\gamma_2^L \neq 0$, the curvature representation can be simplified as follows:

$$\begin{aligned}\text{Cur}(\tau) &\approx \left(\frac{2\gamma_1^L \sigma^3 \text{Cov}(T, L_T) + 3\sigma^2 \text{Cov}(T, L_T^2) + 2\bar{\mu} \text{Cov}(T, L_T^3) - 6\sigma^2 \bar{\mu} E T E[TL_T]}{6\sigma^5 (ET)^{\frac{5}{2}} \sqrt{\tau}} \right) \\ &\quad - \left(\frac{\sigma^4 V(T)}{4\sigma^5 \sqrt{\tau} (ET)^{\frac{5}{2}}} + \frac{6\sqrt{\tau}}{\sqrt{ET}} \psi(\tau)^2 \right) + \left(\frac{\gamma_2^L}{12\sigma (ET)^{\frac{3}{2}} \sqrt{\tau}} \right),\end{aligned}\tag{14}$$

where the first term is $O(\tau^{-1})$, the second term is $O(1)$ and the third term is $O(\tau^{-2})$ as $\tau \rightarrow 0$. The approximation is symmetric with respect to leverage.

Remark 5 In the absence of leverage, the curvature simplifies to

$$\text{Cur}(\tau) \approx \frac{6\sigma^2 \text{Cov}(T, L_T^2) + 4\bar{\mu} \text{Cov}(T, L_T^3) - 3\sigma^4 V(T)}{12\sigma^5 (ET)^{\frac{5}{2}} \sqrt{\tau}} + \frac{\gamma_2^L}{12\sigma (ET)^{\frac{3}{2}} \sqrt{\tau}},$$

where the first fraction becomes immune of τ while the second term still decays. Additionally, the first term relates to the impact of covariance, and the second term relates to the impact of jumps.

For the proof of Proposition 5 and Remark 5, see Appendix F.

From Proposition 5, it follows that the (absolute value of the) ATM curvature increases with the vol-of-vol parameter since both the covariance term and the variance $V(T)$ are quadratic in vol-of-vol.

The kurtosis of the base Lévy process also increases the curvature but decays rapidly at the rate of τ^{-2} . However, the combination of volatility, skewness, and kurtosis can produce flexible decay rates for the curvature across the entire volatility surface. Consequently, the introduction of jumps aids not only in fitting performance at short maturities but also in enhancing the flexibility of the entire volatility term structure.

Corollary 2 Consider a continuous GSVM where v is a diffusion process. The expression for curvature can be further simplified as:

$$\text{Cur}(\tau) \approx \frac{\text{Cov}(T, B_T^2 - T)}{2(ET)^{\frac{5}{2}} \sqrt{\tau}} + \frac{V(T)}{4(ET)^{\frac{5}{2}} \sqrt{\tau}} - \frac{3 \text{Cov}(T, B_T)^2}{2\sqrt{\tau}(ET)^{\frac{7}{2}}}.$$

Furthermore, the ATM curvature is quadratic in ρ and immune of τ for short maturities:

$$\lim_{\tau \rightarrow 0+} \text{Cur}(\tau) = \frac{\gamma(v_0)^2}{24v_0^{\frac{5}{2}}} (2 - 5\rho^2).$$

Under the assumption of Corollary 2, leverage affects the curvature primarily through the correlation between T and B_T^2 . The impact is symmetric, and the curvature is likely to be negative for large $|\rho|$. This phenomenon will also be corroborated by numerical experiments.

Example 6 (Heston) Consider a Heston model. The ATM curvature takes the limit form

$$\lim_{\tau \rightarrow 0+} \text{Cur}(\tau) = \frac{\eta^2}{24v_0^{\frac{3}{2}}} (2 - 5\rho^2).$$

This result is consistent with the findings in [Alos and León \(2017\)](#).

Remark 6 *From Corollary 2, the ATM curvature is quadratic in ρ for time-changed Brownian models. Additionally, we identify a critical value of leverage, $\rho = -\sqrt{0.4}$. Beyond this critical leverage, the curvature can become negative.*

5 Numerical Results

In this section, we conduct an in-depth numerical analysis of diffusion models, focusing on the effects of leverage, vol-of-vol, skewness of the base process, and time to maturity on the volatility skew and curvature. Subsequently, we extend this analysis to jump models. Our study encompasses several widely recognized model specifications, including the Heston model, CGMY jump Heston model ([Carr et al. \(2002\)](#), [Carr et al. \(2003\)](#), [Kim et al. \(2009\)](#)), Merton's jump diffusion ([Merton \(1976\)](#)), and stochastic affine jump diffusion ([Duffie et al. \(2000\)](#)). For a comprehensive examination of CGMY jump models, which are prevalent in derivatives pricing, refer to [Ballotta and Rayée \(2022\)](#). Rough volatility models, which exhibit exploding effects similar to jump models, are not incorporated in the numerical examples. Readers may refer to [Gatheral et al. \(2018\)](#), [El Euch and Rosenbaum \(2019\)](#), and [Guyon \(2021\)](#) for the corresponding experiments, where the observed exploding ATM skew aligns with our approximation results.

The following is the affine jump-diffusion specification of an SVM:

$$\begin{cases} X_t = -(\Psi(-i)v_t + \tilde{\Psi}(-i))dt + \sigma dW(T_t) + \sigma_J dJ(T_t) + \tilde{\sigma}_J d\tilde{J}(t), \\ dv_t = \kappa(\theta - v_t)dt + \eta dW^T(T_t) - \eta_J dJ^T(T_t) + \tilde{\eta}_J d\tilde{J}^T(t), \end{cases} \quad (15)$$

where the time change $T_t = \int_0^t v_s ds$, $dW_t dW_t^T = \rho dt$, J, J^T are pure jump Lévy processes, and J^T only has negative jumps. Meanwhile,

$$\Psi(u) = -\frac{u^2}{2}\sigma^2 + \varphi_J(\sigma_J u),$$

where φ_J is the characteristic exponent of J . Additionally, $\tilde{\Psi}(u) = \varphi_{\tilde{J}}(\tilde{\sigma}_J u)$. Specifically,

- When $\sigma_J = \eta_J = \tilde{\sigma}_J = \tilde{\eta}_J = 0$ and $\sigma = 1$, Equation (15) reduces to the Heston model.
- When

$$\sigma = \eta = \tilde{\sigma}_J = \tilde{\eta}_J = 0 \quad (16)$$

and J, J^T are independent CGMY processes, it results in the unleveraged jump Heston model proposed by [Ballotta and Rayée \(2022\)](#), referred to as model II.

- When

$$\sigma = \eta = \tilde{\sigma}_J = \tilde{\eta}_J = 0, \quad J^T = J^- \quad (17)$$

for CGMY processes J, J^T , we obtain a leveraged jump Heston model.

- When

$$\begin{aligned} \sigma = \eta = \kappa = \eta_J = \sigma_J = \tilde{\eta}_J = 0, \\ \tilde{J} = \sum_{i=1}^N Z_i, N \sim \text{Pois}(\lambda), Z \sim N(\mu, \delta^2), \end{aligned} \quad (18)$$

this corresponds to Merton's pure jump model.

- When

$$\begin{aligned} \sigma = \eta = \sigma_J = \eta_J = 0, \tilde{\sigma}_J = \tilde{\eta}_J = 1, \tilde{J} = \sum_{i=1}^N Z_i, \tilde{J}^T = \sum_{i=1}^N Y_i \\ N \sim \text{Pois}(\lambda), Y \sim \exp(\mu_v), Z \mid (Y = y) \sim N(\mu_S + \rho_J y, \delta^2), \end{aligned} \quad (19)$$

we obtain an affine pure jump model.

5.1 Heston Model

The approximation for the IVS of diffusion models takes the following form:

$$v(k, \tau) \approx \frac{s}{\sqrt{\tau}} + \frac{\gamma_1}{6\sqrt{\tau}}k + \left(\frac{\gamma_2 - 2\gamma_1^2}{24s\sqrt{\tau}} \right) k^2. \quad (20)$$

Figure 1 compares the quality of the approximations and explores the impact of different parameters on the volatility skew. The relevant quantities are computed using the Laplace transform of X_τ . As defined,

$$s^2 = \kappa_2 = K^{(2)}(0), \quad \lambda_1 = \frac{\kappa_3}{(\kappa_2)^{\frac{3}{2}}} = \frac{K^{(3)}(0)}{(K^{(2)}(0))^{\frac{3}{2}}}, \quad \lambda_2 = \frac{\kappa_4}{(\kappa_2)^2} = \frac{K^{(4)}(0)}{K^{(2)}(0)}, \quad (21)$$

where $K(u) = \log E[e^{uX_\tau}]$, the cumulant generating function, is explicit for the Heston model. Numerical differentiations yield s, γ_1 , and γ_2 .

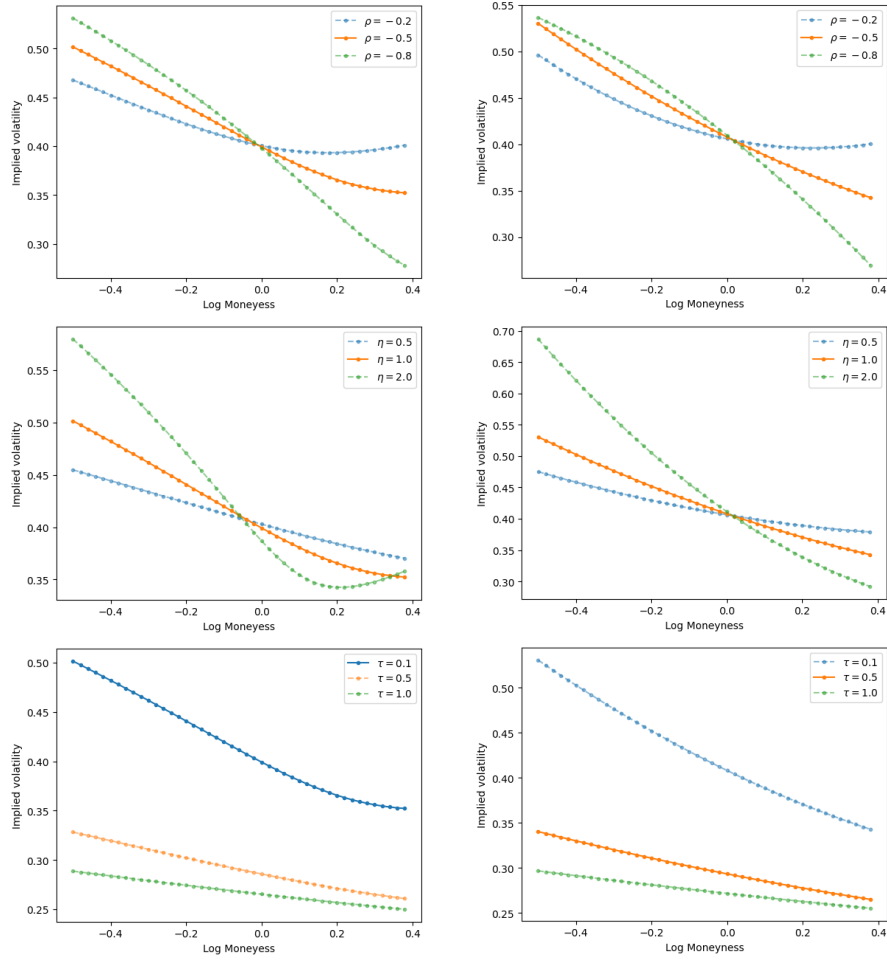


Figure 1: The effect of ρ, η, τ on volatility skew. The left column is the theoretical IVS of Heston model and the right column is the quadratic approximation of IVS by equation (20). The default parameters (shown by solid lines in the plots) are $\kappa = 20, \theta = 0.06, \eta = 1, \rho = -0.5, v_0 = 0.3$.

Observations from figure 1 include:

- Volatility skew increases as ρ becomes more negative or as the vol-of-volatility rises.
- Volatility skew decreases with maturity.
- The approximation formula (20) is satisfactory over a broad range of moneyess ($[-0.5, 0.4]$) and maturity ($[0.1, 1]$).

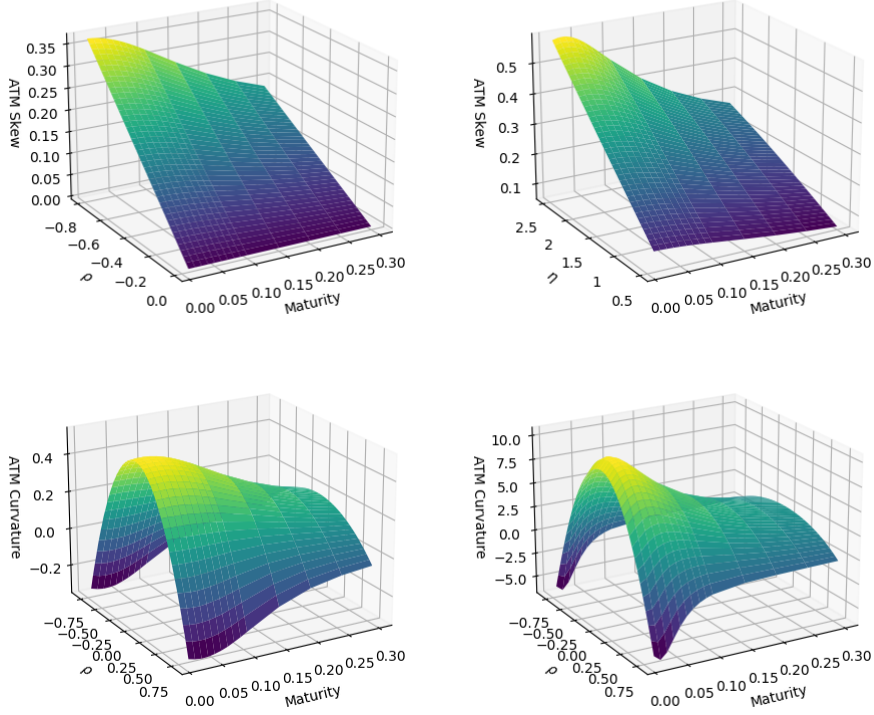


Figure 2: Term structure of ATM volatility skew (first row) and curvature (second row). The same default parameters as in figure (1) is used. The bottom left plot corresponds to vol of vol $\eta = 1$ and the bottom right plot $\eta = 4$. The ATM skew and curvature are plotted for $0.001 \leq \tau \leq 1$.

In figure 2, it is observed that:

- ATM skew and curvature decrease with maturity.
- ATM skew and curvature converge to a constant as $\tau \rightarrow 0$.
- The limiting volatility skew is linearly related to ρ and η .
- Smaller values of $|\rho|$ and η lead to faster convergence of ATM skew and curvature.
- The impact of ρ on ATM curvature is symmetric, and ATM curvature decreases with $|\rho|$.
- When $\rho = -\sqrt{0.4}$, the limiting curvature is close to zero.

- As the vol-of-volatility increases, the ATM curvature converges slowly.

These observations align well with the theoretical results of Proposition 3, Corollary 2, and Example 6.

Next, we test the quality of various approximations of IV. We already have the model-free approximation formula (20), where we have used three parameters in the quadratic function to determine the shape. A rougher approximation based on Heston parameters is given by:

$$v(k, \tau) \approx \text{RV} + \frac{\rho\eta}{4\sqrt{v_0}}k + \frac{\eta^2(2 - 5\rho^2)}{48v_0^{\frac{3}{2}}}k^2, \quad (22)$$

a result from Proposition 3 and Example 6. Here,

$$\text{RV} := \sqrt{ET} = \sqrt{\theta + \frac{(v_0 - \theta)(1 - e^{-\kappa\tau})}{\kappa\tau}}$$

represents the ATM volatility. A variant of the Heston-based formula is also considered where the convexity adjustment is omitted. That is, instead of using $\frac{\gamma_2 - 2\gamma_1^2}{24}$, we adopt $\frac{\gamma_2}{24}$ for quadratic coefficients.

$$v(k, \tau) \approx \text{RV} + \frac{\rho\eta}{4\sqrt{v_0}}k + \frac{\eta^2(1 + 2\rho^2)}{24v_0^{\frac{3}{2}}}k^2, \quad (23)$$

This approximation has been taken in several previous works, e.g. Corrado and Su (1996), Jurczenko et al. (2004), Zhang and Xiang (2008).

(a): With Convexity Adjustment (b): Without Convexity Adjustment

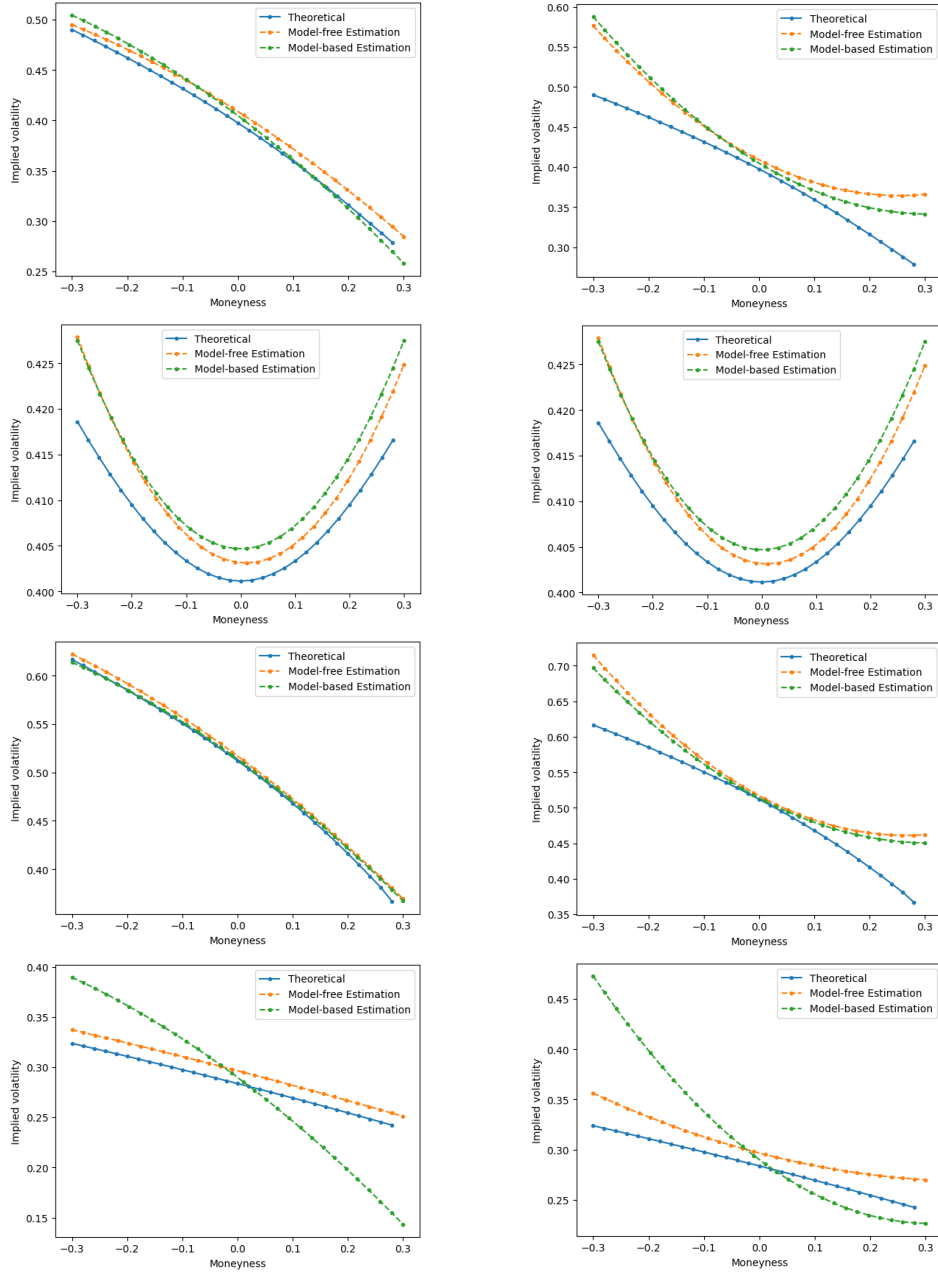


Figure 3: Comparison of the accuracy of the approximations. Column (a) employs the approximations in this work, while column (b) uses approximations without convexity adjustment as in [Corrado and Su \(1996\)](#), [Jurczenko et al. \(2004\)](#), [Zhang and Xiang \(2008\)](#). The first row is based on default parameters with $\rho = -0.9$. The second row is for $\rho = 0$. The third row corresponds to $\tau = 1/60$, and the last row is for $\tau = 0.5$.

From figure 3, it is evident that the convexity adjustment is crucial, particularly in the presence of leverage, where the curvature sign in the volatility smirk may invert. However, in the absence of leverage, the adjustment is unnecessary.

Furthermore, both the model-free formula (20) and the Heston-based formula (22) provide reasonably good approximations. The accuracy of these approximations improves as τ diminishes. Nevertheless, formula (22) tends to overestimate volatility skew as τ increases.

Motivated by these findings and the accuracy of the approximations, parameters η and ρ can potentially be derived from the shape of the short-maturity IVS. The effectiveness of this calibration approach will be validated using real data in section 6.

5.2 Jump-diffusion Models

We investigate the of jumps on the smile using various jump models, specifically models (16), (17), (18), (19).

Remark 7 *In contrast to diffusion models, both γ_1 and γ_2 explode as $\tau \rightarrow 0$, and the additional terms in equation (3) cannot be disregarded. A more accurate approximation can be found in formula (4). We continue to use the original approximation, but highlight the deviation it creates in jump models. A comparison with approximation (4) is shown in Appendix H.2.*

Figure 4 compares the volatility smiles of models (16), (18) and (19) with the corresponding approximation based on formula (20). Due to the rapid change in curvature in jump models, we consider a small moneyness range of $[-0.2, 0.2]$. For model (18), we calculate s , γ_1 , and γ_2 using the following analytic formula:

$$\begin{aligned} s^2 &= (\sigma_J^2 + \lambda\delta^2 + \lambda\mu^2)\tau, \\ \gamma_1 &= \frac{\lambda(3\delta^2\mu + \mu^3)}{(\sigma_J^2 + \lambda\delta^2 + \lambda\mu^2)^{3/2}}, \\ \gamma_2 &= \frac{\lambda(3\delta^4 + 6\mu^2\delta^2 + \mu^4)}{(\sigma_J^2 + \lambda\delta^2 + \lambda\mu^2)^2}. \end{aligned}$$

Explicit formulas for models (16), (17) and (19) do not exist. However, similar to Heston, the cumulant generating function is available for affine models like models (16), (17) and (19). Hence, we compute the quantities s , γ_1 , and γ_2 based on (21).

First, we investigate the effect of jumps on volatility skew. The skewness of a CGMY distribution is given by

$$\frac{C(M^{Y-3} - G^{Y-3})\Gamma(3-Y)}{(C(M^{Y-2} + G^{Y-2})\Gamma(2-Y))^{3/2}}.$$

Since $Y < 2$, as the parameter M increases, the jump component becomes more skewed, resulting in a more negatively skewed smile. Similarly, we control the volatility skew of model (18) and (19) by adjusting parameters δ and ρ_J , respectively.

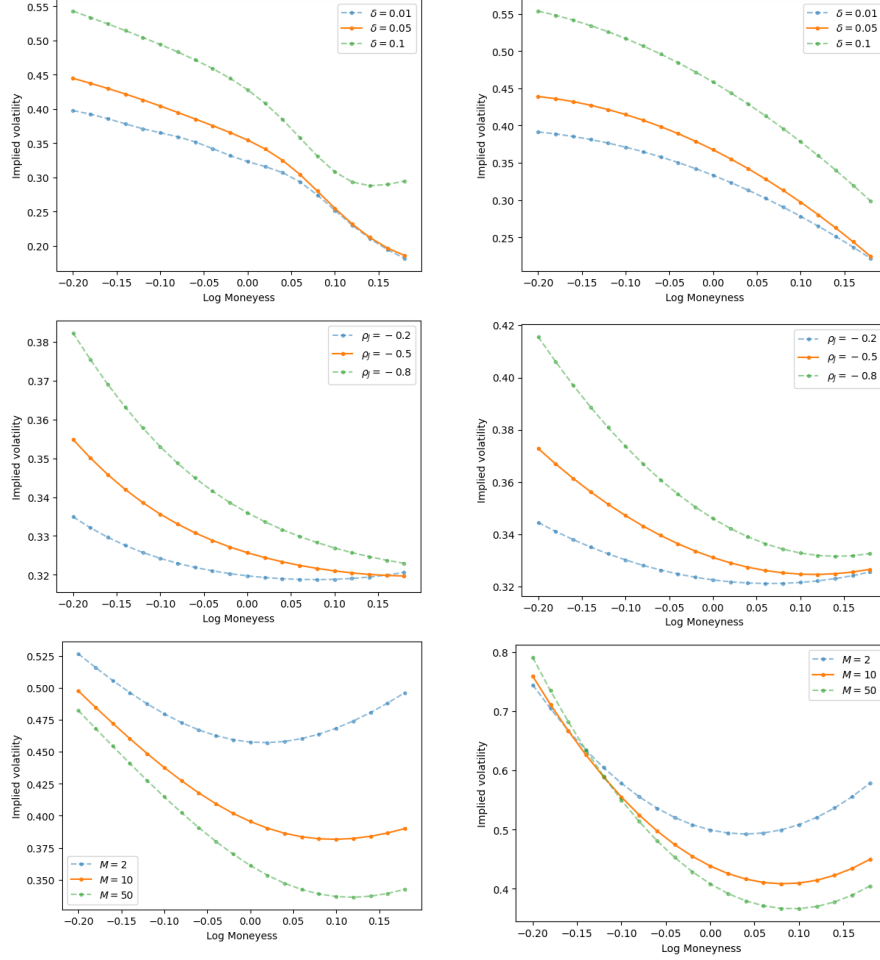


Figure 4: Impact of jump parameters on volatility skew and comparison of model IVS and approximated IVS. The left column shows the true IVS of models (16), (18), (19), while the right column presents a quadratic approximation based on (20). The first row corresponds to model (18) with default parameters $\tilde{\sigma}_J = 0.1, \mu = -0.1, \delta = 0.05, \lambda = 10, v_0 = 0.04$. The second row corresponds to model (19) with default parameters $\kappa = 2, \theta = 0.06, \rho_J = -0.5, \mu_v = 0.05, \mu_S = 0, \delta = 0.01, \lambda = 10, v_0 = 0.1$. The third row corresponds to model (16) with parameters $\kappa = 20, \theta = 0.06, v_0 = 0.1, \sigma_J = 0.5, \eta_J = 0.5, C = 5, G = 1, M = 10, Y = 1.5$.

As noted in Proposition 5, the volatility skew of jump models arises from both leverage and skewness of jumps. We observe the following features.

- When the jumps become more skewed (as indicated in the first and third rows, models (19) and (16), or as leverage increases (as depicted in second row, model (18)), the IVS becomes more skewed.
- The quadratic approximation is relatively satisfactory for models (18) and (19), but exhibits a substantial deviation for model (16).

The results are consistent with Proposition 2. The accuracy of the approximation can be attributed to the choice of jumps. Since models (18) and (19) feature compound Poisson jumps with normal distributions, the jump density decays quickly, resulting in relatively small γ_2 and high-order cumulants. Conversely, in model (16), the CGMY distribution features heavy tails and large kurtosis. The ATM curvature also varies rapidly with moneyness for model (16).

Concerning curvature, unlike leverage and volatility of volatility, γ_2^L explicitly impacts the smile curvature. The excess kurtosis of a CGMY distribution is given by

$$\frac{C (M^{Y-4} + G^{Y-4}) \Gamma(4 - Y)}{(C (M^{Y-2} + G^{Y-2}) \Gamma(2 - Y))^2}$$

and is mainly controlled by parameter C . However, since the variance of L also influences the smile curvature and has the value

$$C (MY - 2 + GY - 2) \Gamma(2 - Y),$$

to maintain the variance invariant, we simultaneously adjust the parameters σ_J and η_J such that the products $\sigma_J^2 C$ and $\eta_J^2 C$ remain constant.

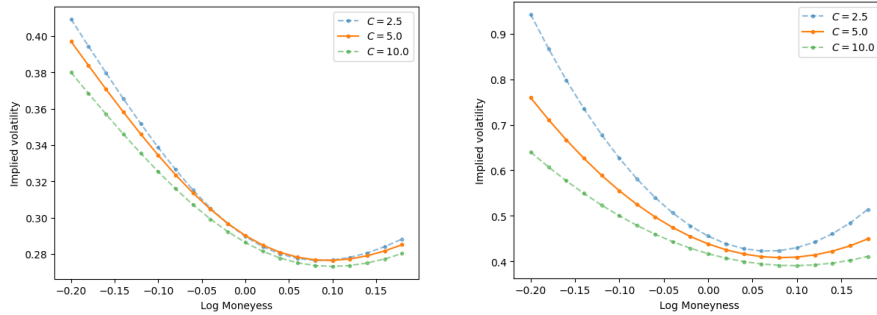


Figure 5: Impact of jump parameters on ATM curvature with default parameters $\kappa = 20, \theta = 0.06, v_0 = 0.3, \sigma_J = 1, \eta_J = 2, G = 0.5, M = 10, Y = 1.5$. The left plot shows the true IVS of model (16), and the right plot presents a quadratic approximation based on formula (20).

The curvature increases for smaller values of C , although the effect is not substantial. Moreover, the approximation is evidently not as accurate as in Heston models. In the appendix, it is shown that formula (4) enhances the approximation to some extent.

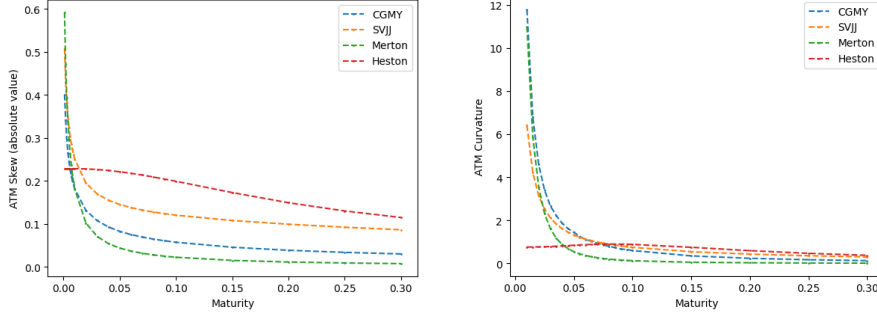


Figure 6: Term structure of ATM skew and curvature of model (16). The left plot shows the ATM volatility skew versus time to maturity from $T = 0.001$ to $T = 1$. The right subplot presents the ATM curvature versus time to maturity from $T = 0.01$ to $T = 1$.

From figure 6, we observe that both the ATM skew and curvature explode as τ approaches 0. Moreover, the rate of explosion increases with the corresponding parameters. This observation highlights the differences between jump-diffusion models and diffusion models.

6 Empirical Application

In this section, we validate effectiveness of the approximations using real market data. We test how a quadratic function of log-moneyness fits the real IVS and the accuracy of the moment-based approximations (5) and (6). Additionally, we present the term structure of the IVS and the associated decay of the approximation accuracy. Finally, we apply the results of the model-based approximation to the calibration problem.

6.1 Data Processing

We use the S&P 500 (SPX) options data as of January 20, 2023. The corresponding maturities range from 9 days to 364 days. We derive the risk-free rates from the daily US Treasury yield curve rates using cubic spline interpolation. Following the standard procedure, we consider only out-of-the-money options and calculate the

forward price through put-call parity:

$$F_0(\tau) = K + e^{r\tau}(C(K, \tau) - P(K, \tau)),$$

where K minimizes $|\frac{Ke^{-r\tau}}{S_0} - 1|$. The log-moneyness for any option is then $k = \log(\frac{K}{F_0(\tau)})$, as defined before.

6.2 Fitting the IVS

We fit the IVS on 01/20/2023 with maturity on 02/17/2023, i.e. $\tau = 28/365$. The function is assumed to be

$$IV(k) = ak^2 + bk + c.$$

Consistent with the approach of [Zhang and Xiang \(2008\)](#), we ensure that the at-the-money implied volatility is accurately captured by setting $c = IV^{\text{mkt}}(\tilde{k})$, where \tilde{k} is chosen closest to 0. We then optimize the following error function:

$$L = \frac{\sum_k \text{Volume} \cdot (IV - IV^{\text{mkt}})^2}{\sum_k \text{Volume}},$$

which is a volume-weighted squared error.

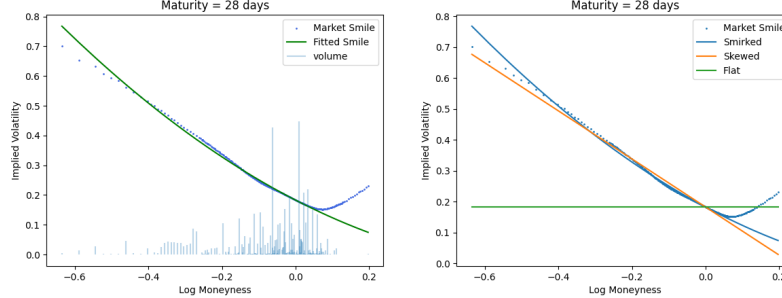


Figure 7: The fitted quadratic function of log-moneyness.

	Weighted RMSE	Weighted MAE	RMSE	MAE
Smirk	0.00898	0.00454	0.02953	0.01360
Skew	0.02406	0.01148	0.04041	0.02286
Flat	0.11219	0.06734	0.12459	0.08040
Spread	0.00485	0.00270	0.00676	0.00387

Table 1: Errors of the fitted smile.

Based on the shape information, such as volatility skew and curvature, we can derive the implied skewness and curvature for the log return as follows:

$$s = c\sqrt{\tau}, \gamma_1 = 6b\sqrt{\tau}, \gamma_2 = 24ac\tau + 72b^2\tau. \quad (24)$$

Estimating these requires considering the “maturity error.” In comparison, the moments recovered from the implied volatility expansion (4) exhibit smaller errors. Table 2 compares the two sets of estimations (3) and (4).

Log Return Shape	Standard deviation	Skewness	Excess Kurtosis
Estimator A	0.05052	-1.05866	2.39163
Estimator B	0.054120	-1.05761	2.40191
Relative	6.64%	0.10%	0.43%

Table 2: Estimator A refers to the first-order estimation of log return shape. They are directly obtained from coefficients a, b, c as in (24). Estimator B is obtained by minimizing the volume-weighted squared error with the IVS expansion (4).

The first-order approximations of skewness and excess kurtosis are indeed accurate for a maturity of one month. We also evaluate the performance at other maturities.

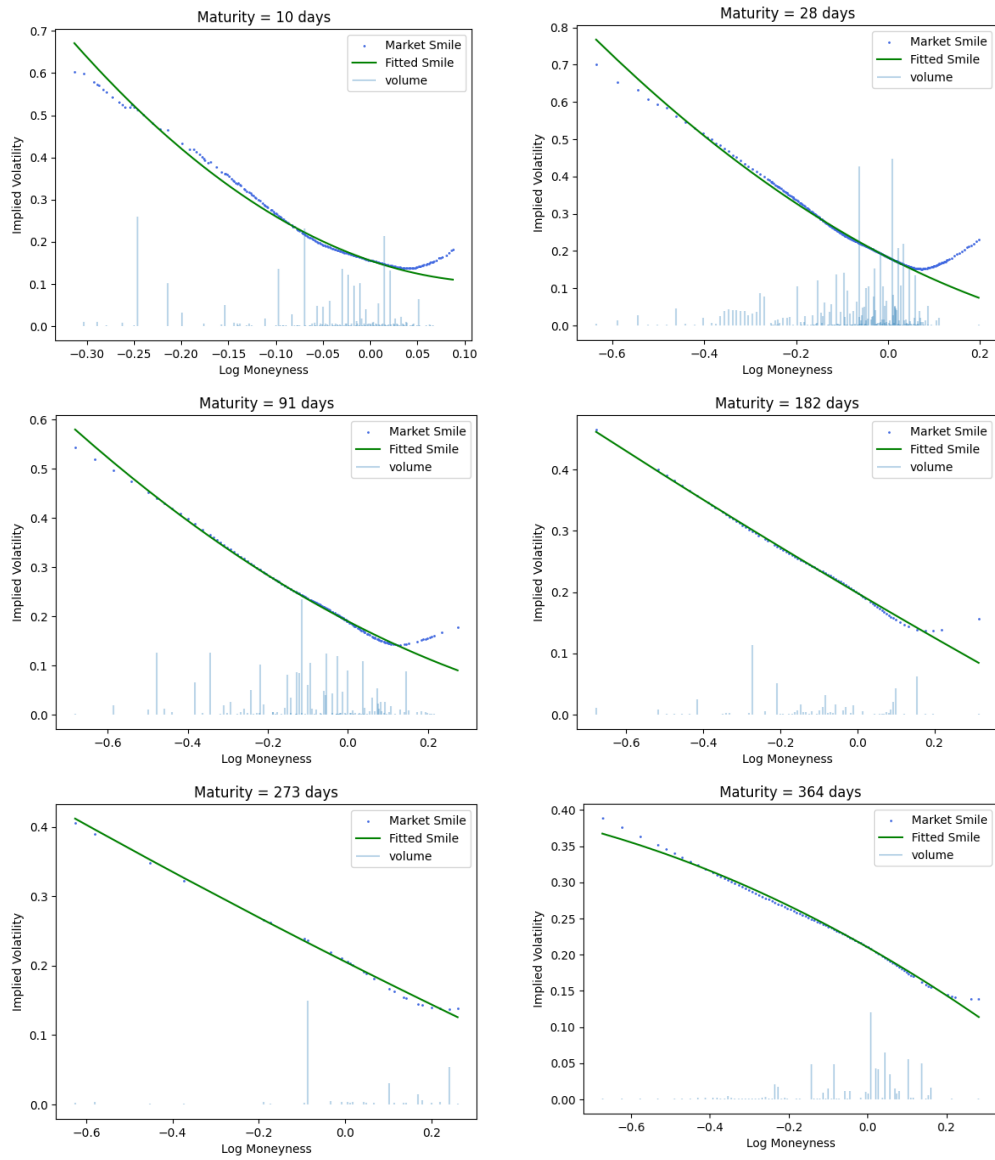


Figure 8

Maturity	Weighted RMSE	Weighted MAE	RMSE	MAE
10 Days	0.00872	0.00579	0.01880	0.01271
28 Days	0.00898	0.00454	0.02953	0.01360
91 Days	0.00551	0.00329	0.01339	0.00591
182 Days	0.00470	0.00296	0.00900	0.00357
273 Days	0.00511	0.00467	0.00567	0.00461
364 Days	0.00258	0.00169	0.00541	0.00340

Table 3: Error of fitted smile.

Maturity	Std	Skewness	Kurtosis	R.E. Std	R.E. Skewness	R.E. Kurtosis
10 Days	0.02573	-0.75948	1.44139	4.61%	0.84%	0.14%
28 Days	0.05052	-1.05866	2.39163	6.64%	0.10%	0.43%
91 Days	0.09463	-1.26887	3.46658	9.12%	3.44%	6.93%
182 Days	0.14023	-1.56926	4.98710	11.42%	7.67%	15.08%
273 Days	0.17794	-1.62472	5.37467	14.55%	10.19%	18.51%
364 Days	0.20989	-1.85531	6.31443	14.06%	8.02%	16.92%

Table 4: The approximations of shape quantities. R.E. refers to relative error.

Improvements are observed in the fitting performance as maturity increases, however, the percentage error of the moment also increases. The smile curvature transitions from being less convex to potentially concave with increasing maturity. Table 4 further illustrates that while the absolute value of volatility skew and curvature diminish with maturity, the skewness and kurtosis of log returns expand.

6.3 Calibration to the IVS

We investigate the calibration to volatility smiles using readily available shape information. The calibration procedure is discussed employing the Heston model. From the implied volatility smile, we identify the ATM volatility v , the ATM skew $\psi(\tau)$, and the ATM curvature $\text{Cur}(\tau)$. An approximation for the ATM volatility is given by $v^2 \approx \frac{ET}{\tau}$.

Furthermore, according to Proposition 3, we have

$$\psi(\tau) = b \approx \frac{\rho\eta}{4v}.$$

The short-term approximation for curvature from Example 6 yields

$$\text{Cur}(\tau) = 2a \approx \frac{\eta^2}{24v^3}(2 - 5\rho^2).$$

Substituting $\tau = 28/365$ leads to the values $(\eta, \rho) \approx (0.778, -0.597)$.

In order to assess the stability of the approximation, we estimate the parameters for all short-term weekly SPX options.

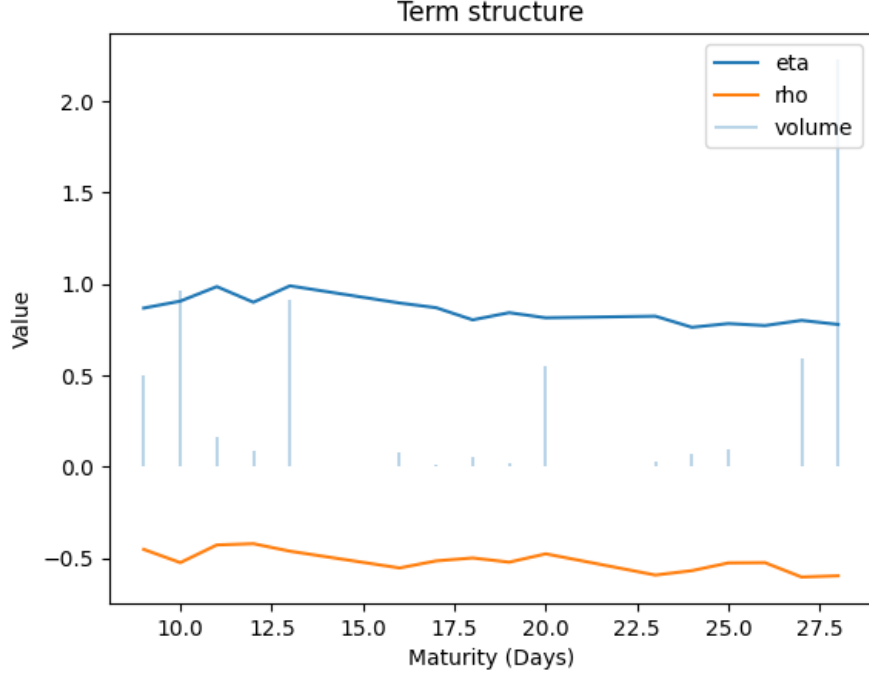


Figure 9: Estimation of η and ρ .

The results are depicted in Figure 9, showing a relatively stable estimation over one month. We then compute a volume-weighted average estimation of $(\eta, \rho) \approx (0.849, -0.536)$. Due to the insignificant size of the ATM skew in explaining the whole volatility skew, particularly in deep OTM cases, a conservative estimation of the volatility skew is developed:

$$\psi(\tau) = 2a \cdot (-0.2) + b = \frac{\rho\eta}{4v},$$

where the moneyness -0.2 signifies the volatility skew in the OTM scenario. The resulting parameters are illustrated in Figure 10.

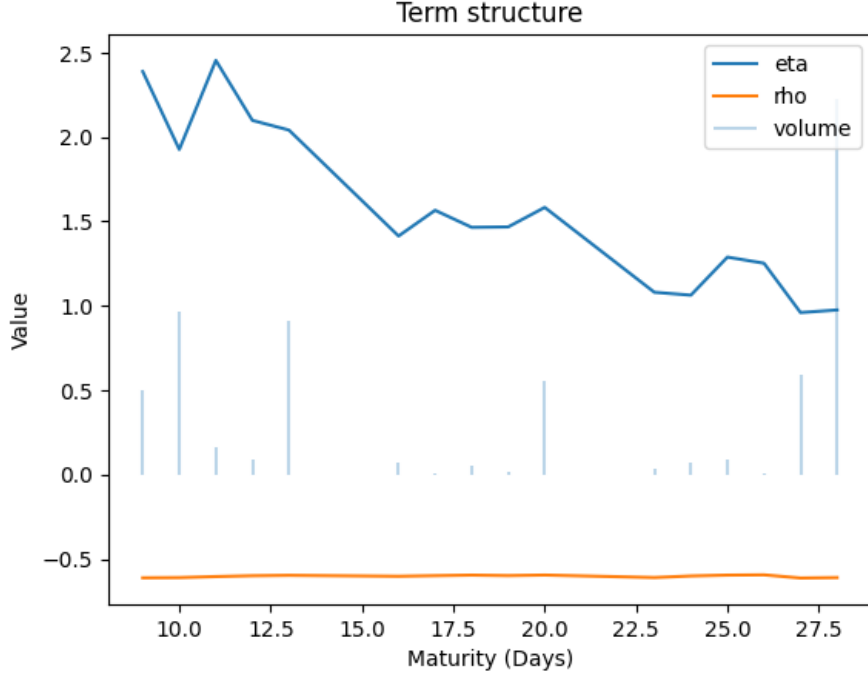


Figure 10: Estimation of η and ρ with conservative volatility skew.

A decrease in the estimated η is observed, as expected due to the sharper short-term volatility skew. However, the leverage parameter ρ remains surprisingly stable.

To evaluate the accuracy of the parameters, calibration is performed on options with maturities ranging from 9 to 28 days utilizing a numerical pricing method. The results are presented in Table 5.

Parameters	η	ρ	κ	θ	v_0	RMSE
ATM Estimation	0.849	-0.536	15	0.1	0.0237	0.02837
OTM Estimation	1.564	-0.602	15	0.1	0.0237	0.02569
Random Start (a)	2.385	-0.071	15	0.1	0.0260	0.0311
Random Start (b)	0.616	-0.610	15	0.1	0.0031	0.0544
Random Start (c)	0.555	-0.376	15	0.1	0.0092	0.0538
Random Start (d)	2.668	-0.591	15	0.1	0.0438	0.0273
Random Start (e)	0.888	-0.509	15	0.1	0.0193	0.0291

Table 5: Comparison of model Calibration under different sets of initial parameters. The random parameters are uniformly sampled as follows: $\eta \in (0, 3)$, $\rho \in (-1, 0)$ and $v_0 \in (0, 0.05)$. The optimizing procedure consists of 50 iterations each.

The sensitivity of the calibration problem to initial parameters and susceptibility to local minima are well-known issues. Therefore, utilizing easily obtained estimates of certain parameters from volatility shapes as initial approximations is advantageous.

7 Conclusion

In this paper, we employ two approximation methods for modeling the shape of the volatility surface.

In the model-free method, we present the moment-based approximation for the ATM skew and curvature. We establish conditions ensuring the convergence of the error to zero, which are applicable to continuous models such as stochastic volatility models and rough volatility models.

Concerning the model-based approach, we derive approximation outcomes for ATM skew and curvature within a time change framework. We provide limit expressions as the maturity approaches zero for stochastic volatility models and rough volatility models. Additionally, we analyze features like the leverage effect and decay rates and suggest their influence on model selection.

Numerical illustrations confirm the efficacy of both model-free and model-based approximation techniques. Furthermore, empirical data from the S&P 500 index exhibit a satisfactory fit of the smile using the quadratic approximation with both skew and curvature. Finally, calibration experiments indicate a potential application of using the approximation results as initial estimates for the calibration issue.

Based on our methods, some properties of the IVS can be obtained for three families of models, as outlined in Table 6.

Table 6: Properties of volatility surface under different classes of models.

Model Property	Diffusion	Jump diffusion	Rough
Short Maturity Skew	Constant	Approximation explodes at order $O(\tau^{-1})$	Approximation explodes at order $O(\tau^{H-\frac{1}{2}})$
Short Maturity Curvature	Constant	Exploding at order $O(\tau^{-2})$	Exploding at order $O(\tau^{2H-1})$
Skew Value	Controlled by leverage & vol-of-vol	Controlled by leverage, vol-of-vol and base process	Controlled by leverage, vol-of-vol and Hurst parameter
Curvature Value	Controlled by leverage & vol-of-vol	Controlled by leverage, vol-of-vol and base process	Controlled by leverage, vol-of-vol and Hurst parameter
Term Structure	Controlled by leverage part only	Controlled by leverage and jump skewness	Controlled by leverage and Hurst parameter
Skew v.s. Leverage	Linear, positive	Non-homogeneous	Linear, positive
Curvature v.s. Leverage	Quadratic, negative	Non-homogeneous	Quadratic, negative
Exactness at Limits	Holds	Generally not	Holds
Examples	Heston (1993); Hull and White (1987); Bergomi (2008)	Duffie et al. (2000); Bates (1996); Carr and Wu (2004); Ballotta and Rayée (2022)	Gatheral et al. (2018); Bayer et al. (2016)

References

- Eduardo Abi Jaber and Omar El Euch. Markovian structure of the volterra heston model. *Statistics & Probability Letters*, 149:63–72, 2019a.
- Eduardo Abi Jaber and Omar El Euch. Multifactor approximation of rough volatility models. *SIAM journal on financial mathematics*, 10(2):309–349, 2019b.
- Yacine Aït-Sahalia, Chenxu Li, and Chen Xu Li. Implied stochastic volatility models. *The Review of Financial Studies*, 34(1):394–450, 2021.
- Elisa Alos and Jorge A León. On the curvature of the smile in stochastic volatility models. *SIAM Journal on Financial Mathematics*, 8(1):373–399, 2017.
- Elisa Alos, Jorge A León, and Josep Vives. On the short-time behavior of the

- implied volatility for jump-diffusion models with stochastic volatility. *Finance and stochastics*, 11(4):571–589, 2007.
- David K Backus, Silverio Foresi, and Liuren Wu. Accounting for biases in black-scholes. *Available at SSRN 585623*, 2004.
- Laura Ballotta and Grégory Rayée. Smiles & smirks: Volatility and leverage by jumps. *European Journal of Operational Research*, 298(3):1145–1161, 2022.
- David S Bates. Jumps and stochastic volatility: Exchange rate processes implicit in deutsche mark options. *The Review of Financial Studies*, 9(1):69–107, 1996.
- Christian Bayer, Peter Friz, and Jim Gatheral. Pricing under rough volatility. *Quantitative Finance*, 16(6):887–904, 2016.
- Henri Berestycki, Jérôme Busca, and Igor Florent. Computing the implied volatility in stochastic volatility models. *Communications on Pure and Applied Mathematics: A Journal Issued by the Courant Institute of Mathematical Sciences*, 57(10):1352–1373, 2004.
- Lorenzo Bergomi. Smile dynamics iii. *Available at SSRN 1493308*, 2008.
- Lorenzo Bergomi and Julien Guyon. Stochastic volatility’s orderly smiles. *Risk*, 25(5):60, 2012.
- Peter Carr and Liuren Wu. What type of process underlies options? a simple robust test. *The Journal of Finance*, 58(6):2581–2610, 2003.
- Peter Carr and Liuren Wu. Time-changed lévy processes and option pricing. *Journal of Financial economics*, 71(1):113–141, 2004.
- Peter Carr, Hélyette Geman, Dilip B Madan, and Marc Yor. The fine structure of asset returns: An empirical investigation. *The Journal of Business*, 75(2):305–332, 2002.
- Peter Carr, Hélyette Geman, Dilip B Madan, and Marc Yor. Stochastic volatility for lévy processes. *Mathematical finance*, 13(3):345–382, 2003.
- Jean-Pierre Chateau, Daniel Dufresne, et al. Gram-charlier processes and applications to option pricing. *Journal of Probability and Statistics*, 2017, 2017.
- Charles J Corrado and Tie Su. Skewness and kurtosis in s&p 500 index returns implied by option prices. *Journal of Financial research*, 19(2):175–192, 1996.
- Darrell Duffie, Jun Pan, and Kenneth Singleton. Transform analysis and asset pricing for affine jump-diffusions. *Econometrica*, 68(6):1343–1376, 2000.

- Omar El Euch and Mathieu Rosenbaum. The characteristic function of rough heston models. *Mathematical Finance*, 29(1):3–38, 2019.
- Omar El Euch, Masaaki Fukasawa, Jim Gatheral, and Mathieu Rosenbaum. Short-term at-the-money asymptotics under stochastic volatility models. *SIAM Journal on Financial Mathematics*, 10(2):491–511, 2019.
- Martin Forde and Antoine Jacquier. The large-maturity smile for the heston model. *Finance and Stochastics*, 15(4):755–780, 2011.
- Martin Forde, Antoine Jacquier, and Roger Lee. The small-time smile and term structure of implied volatility under the heston model. *SIAM Journal on Financial Mathematics*, 3(1):690–708, 2012.
- Peter Friz, Stefan Gerhold, and Arpad Pinter. Option pricing in the moderate deviations regime. *Mathematical Finance*, 28(3):962–988, 2018.
- Jim Gatheral, Thibault Jaisson, and Mathieu Rosenbaum. Volatility is rough. *Quantitative finance*, 18(6):933–949, 2018.
- Héllyette Geman. Pure jump lévy processes for asset price modelling. *Journal of Banking & Finance*, 26(7):1297–1316, 2002.
- Julien Guyon. The smile of stochastic volatility: Revisiting the bergomi-guyon expansion. *Available at SSRN 3956786*, 2021.
- WJ Hall. On wald’s equations in continuous time. *Journal of Applied Probability*, 7(1):59–68, 1970.
- Steven L Heston. A closed-form solution for options with stochastic volatility with applications to bond and currency options. *The review of financial studies*, 6(2):327–343, 1993.
- Jiexiang Huang, Wenli Zhu, and Xinfeng Ruan. Option pricing using the fast fourier transform under the double exponential jump model with stochastic volatility and stochastic intensity. *Journal of Computational and Applied Mathematics*, 263:152–159, 2014.
- John Hull and Alan White. The pricing of options on assets with stochastic volatilities. *The journal of finance*, 42(2):281–300, 1987.
- Robert Jarrow and Andrew Rudd. Approximate option valuation for arbitrary stochastic processes. *Journal of financial Economics*, 10(3):347–369, 1982.

- Emmanuel Jurczenko, Bertrand Maillet*, and Bogdan Negréa. A note on skewness and kurtosis adjusted option pricing models under the martingale restriction. *Quantitative Finance*, 4(5):479–488, 2004.
- Young Shin Kim, Svetlozar T Rachev, Dong Myung Chung, and Michele Leonardo Bianchi. The modified tempered stable distribution, garch-models and option pricing. *Probability and Mathematical statistics*, 29(1):91–117, 2009.
- Steven G Kou. A jump-diffusion model for option pricing. *Management science*, 48(8):1086–1101, 2002.
- Dennis Kristensen and Antonio Mele. Adding and subtracting black-scholes: a new approach to approximating derivative prices in continuous-time models. *Journal of financial economics*, 102(2):390–415, 2011.
- Roger W Lee. The moment formula for implied volatility at extreme strikes. *Mathematical Finance: An International Journal of Mathematics, Statistics and Financial Economics*, 14(3):469–480, 2004.
- Dilip B Madan and Marc Yor. Representing the cgmy and meixner lévy processes as time changed brownian motions. *Journal of Computational Finance*, 12(1):27, 2008.
- Alexey Medvedev and Olivier Scaillet. Approximation and calibration of short-term implied volatilities under jump-diffusion stochastic volatility. *The Review of Financial Studies*, 20(2):427–459, 2007.
- Robert C Merton. Option pricing when underlying stock returns are discontinuous. *Journal of financial economics*, 3(1-2):125–144, 1976.
- Itrel Monroe. Processes that can be embedded in brownian motion. *The Annals of Probability*, pages 42–56, 1978.
- Yasufumi Osajima. The asymptotic expansion formula of implied volatility for dynamic sabr model and fx hybrid model. *Available at SSRN 965265*, 2007.
- Stefano Pagliarani and Andrea Pascucci. The exact taylor formula of the implied volatility. *Finance and Stochastics*, 21(3):661–718, 2017.
- Dacheng Xiu. Hermite polynomial based expansion of european option prices. *Journal of Econometrics*, 179(2):158–177, 2014.
- Jin E Zhang and Yi Xiang. The implied volatility smirk. *Quantitative Finance*, 8(3):263–284, 2008.

Appendix A Proof of Theorem 1 and Proposition 1

The proof of Proposition 1 will assume conditions 1-3 as stated below. Theorem 1 consequently emerges as a byproduct without error analysis.

Step 1: Edgeworth Expansion

Given the density function f of a standardized random variable whose moments of any order exists, the Edgeworth expansion for f is as follows:

$$\begin{aligned} f(x) = & \varphi(x) \left[1 + \frac{\gamma_1}{3!} He_3(x) \right. \\ & + \left(\frac{\gamma_2}{4!} He_4(x) + \frac{10\gamma_1^2}{6!} He_6(x) \right) \\ & + \left(\frac{\gamma_3}{5!} He_5(x) + \frac{\gamma_1\gamma_2}{144} He_7(x) + \frac{\gamma_1^3}{1296} He_9(x) \right) \Big] \\ & + \dots, \end{aligned}$$

where

$$\varphi(x) = \frac{1}{\sqrt{2\pi}} e^{-1/(2x^2)}, \quad x \in \mathbf{R}$$

is the standard normal density, He_k is the Hermite polynomial of order k , and γ_k is the $(k+2)$ -th cumulant. A property of Hermite polynomials is

$$\varphi^{(n)}(x) = (-1)^n He_n(x) \varphi(x).$$

Therefore, the expansion can be approximated by

$$f(x) \approx \varphi(x) - \frac{\gamma_1}{3!} \varphi'''(x) + \left(\frac{\gamma_2}{4!} \varphi^{(4)}(x) + \frac{10\gamma_1^2}{6!} \varphi^{(6)}(x) \right).$$

Before entering into the expansion for option price, we show that the implied volatility is irrelevant to risk-free rate and the dividend yield as long as the moneyness is known.

$$\begin{aligned} C_t(K, T) &\equiv C^{BS}(k_t, K, \tau, v) \\ &= K e^{-r\tau} [\Phi(d_1) - \Phi(d_2)] \end{aligned}$$

where

$$d_1 = \frac{-k_t}{v\sqrt{\tau}} + \frac{1}{2}v\sqrt{\tau}, \quad d_2 = \frac{-k_t}{v\sqrt{\tau}} - \frac{1}{2}v\sqrt{\tau}, \quad \Phi(d) = \frac{1}{\sqrt{2\pi}} \int_{-\infty}^d e^{-\frac{s^2}{2}} ds.$$

Here we denote by $\tau = T - t$ the option time-to-maturity and $k_t = \log(K e^{-(r-\delta)\tau} / S_t) = \log(K/F_t)$ the option moneyness. In many cases, we use the futures price to represent S_t instead of the spot price. Since $C_t(K, T) = e^{-r\tau} E_t[S_T - K]_+$, we have

that the implied volatility is a function of k_t, τ :

$$e^{k_t} \Phi(d_1(k_t, v(k_t, \tau), \tau)) - \Phi(d_2(k_t, v(k_t, \tau), \tau)) = E_t[e^{k_t} - 1]_+.$$

Therefore we assume $r = \delta = 0$ for simplicity.

Step 2: The log return can be standardized as

$$X_\tau = \mu + sX.$$

By the non-arbitrage condition $Ee^{X_\tau} = 1$, we find $\mu = -\ln(E[e^{sX}]) = -\frac{s^2}{2} + O(s^3)$. Utilizing the Edgeworth expansion and the aforementioned assumption, the call price is given by

$$\begin{aligned} C(K, \tau) &= \int_{w^*}^{\infty} (S_0 e^{\mu+sx} - K) f(x) dx \\ &= \int_{w^*}^{\infty} (S_0 e^{\mu+sx} - K) \varphi(x) dx - \frac{\gamma_1}{3!} \int_{w^*}^{\infty} (S_0 e^{\mu+sx} - K) \varphi'''(x) dx \\ &\quad + \frac{\gamma_2}{4!} \int_{w^*}^{\infty} (S_0 e^{\mu+sx} - K) \varphi^{(4)}(x) dx + \frac{10\gamma_1^2}{6!} \int_{w^*}^{\infty} (S_0 e^{\mu+sx} - K) \varphi^{(6)}(x) dx + \epsilon \\ &= S_0 \Phi(d) \left(1 + \frac{\gamma_1}{3!} s^3 + \frac{\gamma_2}{4!} s^4 + \frac{10\gamma_1^2}{6!} s^6\right) - K \Phi(d - s) \\ &\quad + S_0 \varphi(d) \times \left(\frac{\gamma_1}{3!} \sum_{n=2}^3 s^{n-1} H e_{3-n}(s - d) + \frac{\gamma_2}{4!} \sum_{n=2}^4 s^{n-1} H e_{4-n}(s - d) \right. \\ &\quad \left. + \frac{10\gamma_1^2}{6!} \sum_{n=2}^6 s^{n-1} H e_{6-n}(s - d) \right) + \epsilon \end{aligned}$$

with γ_1 the skewness of X_τ , γ_2 the excess kurtosis of X_τ , $w^* = (k - \mu)/s$ and

$$d = \frac{\log(S_0/K) - \mu}{s} = \frac{-k + \frac{s^2}{2}}{s} + O(s^2). \quad (25)$$

Note that

$$\varphi(d) - \varphi\left(\frac{-k + \frac{s^2}{2}}{s}\right) = O(s^2), \quad \Phi(d) - \Phi\left(\frac{-k + \frac{s^2}{2}}{s}\right) = O(s^2),$$

since $\frac{k}{s}$ is uniformly bounded by condition 2. We then substitute d by $\tilde{d} = \frac{-k + \frac{s^2}{2}}{s}$ and introduce an error term $O(s^2)$. Then applying condition 3, substituting (25) into the call price and combining the terms with order equal to or higher than s^2 yield

$$\begin{aligned} C(K, \tau) &= S_0 \Phi(\tilde{d}) - K \Phi(\tilde{d} - s) + S_0 \varphi(\tilde{d}) s \left[\frac{\gamma_1}{3!} \frac{k}{s} + \frac{\gamma_2}{4!} \left(\frac{k^2}{s^2} + 2k - 1 \right) \right. \\ &\quad \left. + \frac{10\gamma_1^2}{6!} \left(\frac{k^4}{s^4} + \frac{3k^3}{s^2} - \frac{6k^2}{s^2} - 9k + 3 \right) \right] + O(s^2) + \epsilon, \end{aligned} \quad (26)$$

where

$$w := s - \tilde{d} = \frac{k}{s} + \frac{s}{2}.$$

The error term ϵ results from truncating the Edgeworth series.

Next, we derive the expression for implied volatility v . By condition 3, $\kappa_n = o(1)$. Then $\gamma_1 \rightarrow 0, \gamma_2 \rightarrow 0$, and the truncation error $\epsilon = o(s)$ as $\tau \rightarrow 0$, we deduce that

$$C(K, \tau) - (S_0 \Phi(d) - K \Phi(d - s)) \rightarrow 0$$

uniformly for $|\frac{k}{s}| \leq M$. The implied volatility v satisfies

$$v\sqrt{\tau} - s \rightarrow 0$$

uniformly since the solution to the BS formula is unique. This justifies a linear approximation around $v = \frac{s}{\sqrt{\tau}}$ as

$$\begin{aligned} C(K, \tau) &= S_0 \Phi[d(v\sqrt{\tau})] - K \Phi[d(v\sqrt{\tau}) - v\sqrt{\tau}] \\ &= S_0 \Phi[d(s)] - K \Phi[d(s) - s] + S_0 \varphi(d(s)) (v\sqrt{\tau} - s) \\ &\quad - S_0 \varphi(d(\tilde{s})) \left(\frac{\tilde{s}}{4} - \frac{k^2}{\tilde{s}^3} \right) \frac{(v\sqrt{\tau} - s)^2}{2}, \end{aligned} \quad (27)$$

where \tilde{s} is some point between s and $v\sqrt{\tau}$,

$$d(x) = \frac{-k + x^2/2}{x}.$$

Mean-value theorem yields

$$\begin{aligned} S_0 \varphi(d(\tilde{s})) (v\sqrt{\tau} - s) &= S_0 \varphi(\tilde{d}) s \left[\frac{\gamma_1}{3!} \frac{k}{s} + \frac{\gamma_2}{4!} \left(\frac{k^2}{s^2} + 2k - 1 \right) \right. \\ &\quad \left. + \frac{10\gamma_1^2}{6!} \left(\frac{k^4}{s^4} + \frac{3k^3}{s^2} - \frac{6k^2}{s^2} - 9k + 3 \right) \right] + o(s). \end{aligned}$$

Therefore we have $v\sqrt{\tau} - s = o(s)$. We then obtain the order of the Taylor's expansion residual as $S_0 \varphi(d(\tilde{s})) \left(\frac{\tilde{s}}{4} - \frac{k^2}{\tilde{s}^3} \right) \frac{(v\sqrt{\tau} - s)^2}{2} = o(s)$. The truncation error can be merged with expansion error because we already know $\epsilon = o(s)$.

A linear approximation for implied volatility is then obtained as

$$\begin{aligned} v(k, \tau) &= \frac{s}{\sqrt{\tau}} \left[1 + \frac{\gamma_1}{3!} \frac{k}{s} + \frac{\gamma_2}{4!} \left(\frac{k^2}{s^2} + 2k - 1 \right) \right. \\ &\quad \left. + \frac{10\gamma_1^2}{6!} \left(\frac{k^4}{s^4} + \frac{3k^3}{s^2} + 4k^2 - \frac{6k^2}{s^2} - 9k + 3 \right) \right] + \epsilon_v \\ &= \frac{s}{\sqrt{\tau}} \left[\left(1 + \frac{\gamma_1^2 - \gamma_2}{24} \right) + \left(\frac{\gamma_1}{6s} + \frac{\gamma_2}{12} - \frac{\gamma_1^2}{8} \right) k + \left(\frac{\gamma_2 - 2\gamma_1^2}{24s^2} \right) k^2 \right] + \epsilon_v \\ &= \frac{s}{\sqrt{\tau}} \left[1 + \frac{\gamma_1}{6s} k + \left(\frac{\gamma_2 - 2\gamma_1^2}{24s^2} \right) k^2 \right] + \epsilon_v, \end{aligned}$$

where $\epsilon_v = o(1)$ contains three parts of error: truncation of Edgeworth series, Taylor expansion residual and those terms containing k^2 or higher orders. As a result, the ATM skew has the leading order approximation

$$\psi(\tau) \approx \frac{\gamma_1}{6\sqrt{\tau}}.$$

Likewise, the ATM curvature admits the leading order approximation

$$\text{Cur}(\tau) \approx \frac{\gamma_2 - 2\gamma_1^2}{12s\sqrt{\tau}}. \quad (28)$$

To assess the accuracy of the approximation for ATM skew and curvature, we identify two sources of error: truncation and linear approximation. The factor in the Edgeworth series influencing ATM skew is the linear term $\frac{k}{s}$ in the high-order Hermite polynomials. Under the condition $\kappa_n = o(\gamma_1)$, the error induced in ATM skew is then of the order

$$\frac{C\kappa_n}{\sqrt{\tau}} = o\left(\frac{\gamma_1}{\sqrt{\tau}}\right), \quad n \geq 5.$$

Moving on to the error caused by linear approximation (27), according to the mean-value theorem, we have $v\sqrt{\tau} - s = O(s\gamma_1)$ and $O(s\gamma_2) = O(s\gamma_1)$ given that $\gamma_2 = O(\gamma_1)$, and $\gamma_n = o(\gamma_2)$ for $n \geq 3$. Consequently, the derivative of the residual of Taylor's expansion becomes of the order $O(s^3\gamma_1^2)$, resulting in an error on ATM skew of $O(\frac{s^3\gamma_1^2}{\sqrt{\tau}})$, a higher order term compared to the main term.

In the case of ATM curvature, it is the quadratic term $\frac{k^2}{s^2}$ in the Hermite polynomials that are significant. The induced error is of the order

$$\frac{C\kappa_n}{s\sqrt{\tau}} = o\left(\frac{\gamma_2}{s\sqrt{\tau}}\right), \quad n \geq 5.$$

To analyze the error of Taylor's expansion, a second-order Taylor expansion is needed:

$$\begin{aligned} C(K, \tau) &= S_0\Phi[d(v\sqrt{\tau})] - K\Phi[d(v\sqrt{\tau}) - v\sqrt{\tau}] \\ &= S_0\Phi[d(s)] - K\Phi[d(s) - s] + S_0\varphi(d)(v\sqrt{\tau} - s) \\ &\quad - S_0\varphi(d)\left(\frac{s}{4} - \frac{k^2}{s^3}\right)\frac{(v\sqrt{\tau} - s)^2}{2} + \epsilon_{BS}, \end{aligned} \quad (29)$$

where ϵ_{BS} has the leading term in k^2

$$\frac{k^2}{\tilde{s}^4}(v\sqrt{\tau} - s)^3,$$

and its second derivative has an order of $O(\frac{\gamma_1^3}{s})$. The error induced in ATM curvature is then of the order $O(\frac{\gamma_1^3}{s\sqrt{\tau}})$, a higher-order term. The solution to the new expansion is

$$v\sqrt{\tau} - s = F(k) := \frac{1 - \sqrt{1 - M(k)(\frac{s}{2} - \frac{2k^2}{s^3})}}{\frac{1}{2}(\frac{s}{2} - \frac{2k^2}{s^3})},$$

where

$$M(k) = s \left[\frac{\gamma_1}{3!} \frac{k}{s} + \frac{\gamma_2}{4!} \left(\frac{k^2}{s^2} + 2k - 1 \right) + \frac{10\gamma_1^2}{6!} \left(\frac{k^4}{s^4} + \frac{3k^3}{s^2} - \frac{6k^2}{s^2} - 9k + 3 \right) \right] + O(s^2)$$

is of order $O(s\gamma_1) + O(s\gamma_2)$. Since $M(k)(\frac{s}{2} - \frac{2k^2}{s^3}) = o(1)$, we may compute the second-order derivative by expanding the term:

$$F(k) = M(k) - \frac{1}{4}M(k)^2 \left(\frac{s}{2} - \frac{2k^2}{s^3} \right) + \epsilon_F,$$

where ϵ_F contains the k term of the order 3 or higher.

The first term is $M(k)$, resulting in the same derivative $M''(k)$ as in Corollary 1. The second term contains a k^2 term $-\frac{1}{8}k^2s\gamma_1^2 + \frac{k^2\gamma_2^2}{2s}$, leading to an error of order $O(\frac{s\gamma_1^2}{\sqrt{\tau}}) + O(\frac{\gamma_2^2}{s\sqrt{\tau}})$ on ATM curvature, again a high-order term. In conclusion, the ATM curvature formula provides a leading-order approximation as long as $\kappa_n = o(\gamma_2)$, $n \geq 5$.

Appendix B Proof of Theorem 2

Since the n -th cumulants of the Heston model satisfy the condition of limiting exactness, we only need to demonstrate that the orders of κ_n for every continuous stochastic volatility model are the same. This is equivalent proving that every moment of B_T is of the same order.

According to Hall (1970), for a time-changed Brownian motion B_T , the expression

$$V_m = B_T^m + \sum_{j=1}^{\lfloor \frac{m}{2} \rfloor} a_{jm} (-T)^j B_T^{m-2j}$$

represents a zero-mean martingale, where $\{a_{jm}\}$ are real constants. First, we consider diffusion stochastic volatility models in a time-change form:

$$dv_t = \mu(v_t)dt + \gamma(v_t)dW_{T_t}.$$

Apply Itô's formula to $\mu(\cdot)$ and $\gamma(\cdot)$, we get:

$$\begin{aligned} v_t - v_0 &= \int_0^t \mu(v_s) ds + \int_0^t \gamma(v_s) dW_{T_s} \\ &= \mu(v_0)t + \gamma(v_0)W_{T_t} + \int_0^t \mathcal{L}\mu(v_s) ds + \int_0^t \mathcal{L}\gamma(v_s) dW_{T_s} \\ &= \gamma(v_0)W_{T_t} + o(dv), \end{aligned}$$

where \mathcal{L} is the infinitesimal generator of v and $dv = v_t - v_0$. Given that V_m is a zero-mean martingale for $m \geq 2$, we have:

$$\begin{aligned} E[B_T^m] &= \sum_{j=1}^{\lfloor \frac{m}{2} \rfloor} (-a_{jm})^{j-1} E[T^j B_T^{m-2j}] \\ &= \sum_{j=1}^{\lfloor \frac{m}{2} \rfloor} (-a_{jm})^{j-1} E \left[\left(v_0\tau + \gamma(v_0) \int_0^\tau W_{T_s} ds + o(T) \right)^j B_T^{m-2j} \right], \end{aligned}$$

whose order does not depend on the choice of $\mu(\cdot)$ and $\gamma(\cdot)$. In addition, the terms with $\int_0^\tau W_{T_s} ds$ are not cancelled out in κ_n for a general value of $\gamma(v_0)$, and the error terms with $o(T)$ always have higher order than the corresponding terms with $\int_0^\tau W_{T_s} ds$. As a result, the orders of cumulants $\kappa_n(B_T)$ are also independent of the choice of $\mu(\cdot)$ and $\gamma(\cdot)$. This implies that they share the same orders as the Heston model.

For rough models of the form

$$v_t = v_0 + \int_0^t K(t-u)\mu(v_u)du + \int_0^t (t-u)^{\alpha-1}\gamma(v_u)dW_{T_u},$$

applying Itô's formula to $\mu(\cdot)$ and $\gamma(\cdot)$, we obtain:

$$v_t - v_0 = \gamma(v_0) \int_0^t (t-s)^{\alpha-1} dW_{T_s} + o(dv)$$

and

$$E[B_T^m] = \sum_{j=1}^{\lfloor \frac{m}{2} \rfloor} (-a_{jm})^{j-1} E \left[\left(v_0\tau + \gamma(v_0) \int_0^\tau \int_0^t (t-u)^{\alpha-1} dW_{T_u} dt + o(T) \right)^j B_T^{m-2j} \right],$$

which also leads to the conclusion that the orders of cumulants of X_τ do not depend on the choice of $\mu(\cdot)$ and $\gamma(\cdot)$.

Finally, we demonstrate that the cumulants of normalized X_τ for rough volatility models satisfy

$$\kappa_n = O(\tau^{(n-2)H})$$

by considering rough Heston models (5). According to [El Euch and Rosenbaum \(2019\)](#), the moment generating function is given by

$$E[e^{uX_\tau}] = \exp(\kappa\theta I^1 h(u, t) + v_0 I^{1-\alpha} h(u, t)),$$

where $h(u, \cdot)$ is solution of the fractional Riccati equation

$$D^\alpha h(u, t) = \frac{1}{2}(u^2 - u) + \kappa(u\rho\nu - 1)h(u, t) + \frac{(\kappa\nu)^2}{2}h^2(u, t), \quad I^{1-\alpha}h(u, 0) = 0,$$

and the fractional derivative D^α and fractional integral I^α are defined as

$$I^r f(t) = \frac{1}{\Gamma(r)} \int_0^t (t-s)^{r-1} f(s) ds,$$

for $r \in (0, 1]$ and

$$D^r f(t) = \frac{1}{\Gamma(1-r)} \frac{d}{dt} \int_0^t (t-s)^{-r} f(s) ds,$$

for $r \in [0, 1)$. By definition, if k is the leading order of the coefficient of u^n , then $\kappa_n(X_\tau) = O(\tau^k)$. $\frac{\partial I^{1-\alpha}h(u, 0)}{\partial t} = D^\alpha h(u, 0)$, as a polynomial function of u , has the highest order term u^2 since $h(u, 0) = 0$. Setting

$$F(u, x) = \frac{1}{2}(u^2 - u) + \kappa(u\rho\nu - 1)x + \frac{(\kappa\nu)^2}{2}x^2,$$

we have $D^\alpha h(u, t) = F(u, h(u, t))$, and by Taylor's expansion for fractional derivatives:

$$F(u, h(u, t)) = \sum_{k=0}^{\infty} \frac{t^{\alpha k}}{(\alpha k)!} (D^\alpha)^k F(u, h(u, 0)).$$

For $k = 1$,

$$\begin{aligned} D^\alpha F(u, h) &= \kappa(u\rho\nu - 1)D^\alpha h(u, t) + \frac{(\kappa\nu)^2}{2}D^\alpha h^2(u, t) \\ &= \kappa(u\rho\nu - 1)F(u, h) + (\kappa\nu)^2 h(u, t)F(u, h) \end{aligned}$$

by the chain rule of fractional derivative. Then $D^\alpha F(u, 0)$ has the highest order term u^3 . By iterative argument,

$$(D^\alpha)^k F(u, 0) = \kappa(u\rho\nu - 1)(D^\alpha)^{k-1} F(u, 0) + \sum_{\substack{s+r=n-1, \\ s \geq 1, r \geq 1}} C_{sr} (D^\alpha)^s F(u, 0) (D^\alpha)^r F(u, 0)$$

for $k \geq 2$. Like the argument in example 3, using an induction approach, we show that $(D^\alpha)^k F(u, 0)$ takes the highest order term u^{k+2} . By integration, the coefficient of u^n in the expansion of $I^{1-\alpha} h(u, t)$ has the order $O(\tau^{(n-2)\alpha+1})$. To deal with $I^1 h(u, t)$, we consider the fractional Taylor expansion for $h(u, t)$. It has been established that $(D^\alpha)^k h(u, 0)$ takes the highest order term u^{k+1} for $k \geq 1$. By integration, the coefficient of u^n in the expansion of $I^1 h(u, t)$ has the equivalent infinitesimal $O(\tau^{(n-1)\alpha+1})$. Consequently, the leading order for $\kappa_n(X_\tau)$ is $(n-2)\alpha + 1$ for $n \geq 1$ and

$$\kappa_n = O(\tau^{(n-2)\alpha+1-\frac{n}{2}}) = O(\tau^{(n-2)H}), \quad n \geq 2,$$

which implies rough models satisfy condition 3. Given that Conditions 1-2 are also satisfied, the limiting equivalence of the approximations holds as a result of Proposition 1.

Appendix C Proof of Theorem 3

Proof We start with Wald's second equation, which gives us

$$\begin{aligned} V(X_\tau) &= E[L_T + \bar{\mu}T]^2 - \mu^2(ET)^2 \\ &= \sigma^2 ET + 2\bar{\mu}ETL_T + \mu^2 V(T) \\ &= \sigma^2 ET + o(\tau). \end{aligned}$$

The last step is because $|ETL_T| \leq \sqrt{V(T)V(L_T)} \leq O(\tau^{\frac{3}{2}})$.¹ Next, we calculate the third moment of X_τ as follows:

$$\begin{aligned} E(X_\tau - EX_\tau)^3 &= E\left(L_T + \bar{\mu}\tilde{T}\right)^3 \\ &= 3\sigma^2 ETL_T + \kappa_3^L ET + 3\bar{\mu}E\left[\tilde{T}L_T(\bar{\mu}\tilde{T} + L_T)\right] + \bar{\mu}^3 E\tilde{T}^3 \\ &= 3\sigma^2 ETL_T + 3\bar{\mu}E[\tilde{T}L_T^2] + \kappa_3^L ET + O(\tau^{\frac{5}{2}}), \end{aligned}$$

where $\tilde{T} = T - ET$ and the last step is because $|E\tilde{T}^2 L_T| \leq \sqrt{V(T^2)V(L_T)} \leq O(\tau^{\frac{5}{2}})$, with $V(T^2) \leq E(\int_0^\tau v_t dt)^4 \leq O(\tau^4)$. Then, the skewness of X_τ is determined by

$$\gamma_1 = \frac{E(X_\tau - EX_\tau)^3}{V(X_\tau)^{\frac{3}{2}}} = \frac{3ETL_T}{\sigma(ET)^{\frac{3}{2}}} + \frac{3\bar{\mu}E[\tilde{T}L_T^2]}{\sigma^3(ET)^{\frac{3}{2}}} + \frac{\gamma_1^L}{\sqrt{ET}} + \epsilon + O(\tau).$$

¹The specific order of ETL_T depends on the model. For Markov SVMs, the order is $O(\tau^2)$, but for rough models, the order ranges from $O(\tau^{\frac{3}{2}})$ to $O(\tau^2)$. The two cases will be discussed in the following propositions.

The error term consists of two components. One is at most $O(\sqrt{\tau})$ and converges to zero as $\tau \rightarrow 0$, while the second component, ϵ , is induced by removing the high-order terms in the denominator and represents the high-order error of the main term. Thus, we have

$$\frac{\gamma_1}{6\sqrt{\tau}} = \frac{\text{Cov}(T, L_T)}{2\sigma\sqrt{\tau}(ET)^{\frac{3}{2}}} + \frac{\bar{\mu} \text{Cov}(T, L_T^2)}{2\sigma^3\sqrt{\tau}(ET)^{\frac{3}{2}}} + \frac{\gamma_1^L}{6\sqrt{\tau}ET} + \epsilon + O(\sqrt{\tau}),$$

where the error term is $O(\sqrt{\tau})$ because γ_1 is divided by the order of $O(\sqrt{\tau})$.

Moving on to the fourth central moment of the TCLP, it can be expressed as:

$$\begin{aligned}\mu_4 &= E(L_T + \bar{\mu}\tilde{T})^4 = EL_T^4 + 4\bar{\mu}E\tilde{T}L_T^3 + 6\bar{\mu}^2E[\tilde{T}^2L_T^2] + O(\tau^{\frac{7}{2}}) \\ &= 6\sigma^2E[TL_T^2] + 4\kappa_3^LE[TL_T] + \kappa_4^LET - 3\sigma^4ET^2 + 4\bar{\mu}E\tilde{T}L_T^3 + 6\bar{\mu}^2E[\tilde{T}^2L_T^2] + O(\tau^{\frac{7}{2}}).\end{aligned}$$

The excess kurtosis of the log return X_τ is then given by:

$$\begin{aligned}\gamma_2 &= \frac{\mu_4}{\mu_2^2} - 3 \\ &= \frac{6\sigma^2ETL_T^2 + 4\kappa_3^LET L_T + \kappa_4^LET - 3\sigma^4ET^2 + 4\bar{\mu}E\tilde{T}L_T^3 + 6\bar{\mu}^2E[\tilde{T}^2L_T^2]}{\sigma^4(ET)^2 + 4\bar{\mu}\sigma^2ETE[TL_T] + o(\tau^3)} \\ &\quad - 3 + O(\tau^{\frac{3}{2}}) \\ &= \frac{6\text{Cov}(T, L_T^2) - 12\bar{\mu}ETE[TL_T]}{\sigma^2(ET)^2} + \frac{4\bar{\mu}\text{Cov}(T, L_T^3) + 6\bar{\mu}^2E[\tilde{T}^2L_T^2]}{\sigma^4(ET)^2} - \frac{3V(T)}{(ET)^2} \\ &\quad + \frac{4\gamma_1^L\text{Cov}(T, L_T)}{\sigma(ET)^2} + \frac{\gamma_2^L}{ET} + O(\tau^{\frac{3}{2}}) + \epsilon.\end{aligned}$$

Finally, the expression for volatility curvature is a direct result of equation (6), where the denominator has the order $O(\tau)$. By division, we obtain the desired form with high-order error.

Moreover, under the cumulant condition, the approximation terms in equations (5) and (6) have the leading effect, indicating that the approximations under the time change framework have leading orders. \square

Appendix D Proof of Proposition 2 and Proposition 3

We demonstrate the decay rate of each term with respect to time to maturity τ . First, we notice that $E\langle L_2, L \rangle_t = \sigma^2 \rho_t t$, then

$$\begin{aligned}
\text{Cov}(T, L_T) &= E \left[\int_0^\tau v_t dt \cdot L_T \right] \\
&= E \left[\left(\int_0^\tau \int_0^t \gamma(v_s) dL_{2,T_s} dt \right) \left(\int_0^\tau 1 dL_{T_t} \right) \right] + o(\tau^2) \\
&= E \left[\left(\int_0^\tau (\tau - t) \gamma(v_t) dL_{2,T_t} \right) \left(\int_0^\tau 1 dL_{T_t} \right) \right] + o(\tau^2) \\
&= E \left[\int_0^\tau (\tau - t) \rho \sigma^2 v_t \gamma(v_t) dt \right] + o(\tau^2) \\
&= \rho \sigma^2 E \left[\int_0^\tau (\tau - t) \gamma(v_t) v_t dt \right] + o(\tau^2) \\
&= O(\tau^2),
\end{aligned}$$

where the third line follows from the stochastic Fubini's theorem and the fourth line from the property of predictable quadratic variation for local martingales. The short-maturity order follows immediately from the integration.

We can also show that

$$\begin{aligned}
V(T) &= E \left(\int_0^\tau (\tau - t) \gamma(v_t) dL_{2,T_t} \right)^2 + o(\tau^3) \\
&= \sigma^2 E \left(\int_0^\tau (\tau - t)^2 v_t \gamma(v_t)^2 dt \right) + o(\tau^3) \\
&= O(\tau^3).
\end{aligned}$$

Meanwhile, the order of $\text{Cov}(T, L_T^2)$ is also equal to or higher than $O(\tau^2)$. Specifically, if $\kappa_3^L \neq 0$, then $\text{Cov}(T, L_T^2) = O(\tau^2)$. To derive this, we assume

without loss of generality that $\gamma(v_0) \neq 0$.

$$\begin{aligned}
\text{Cov}(T, L_T^2) &= E \left[\left(\int_0^\tau (\tau - t) \gamma(v_t) dL_{2,T_t} \right) (L_{T_\tau}^2 - \sigma^2 T) \right] + \sigma^2 V(T) + \epsilon \\
&= \int_0^\tau (\tau - t) \gamma(v_0) d \left(E \left[L_{2,T_t} (\rho L_{2,T_t} + \sqrt{1 - \rho^2} L_{3,T_t})^2 \right] - \sigma^2 E[T_t L_{2,T_t}] \right) \\
&\quad + \sigma^2 V(T) + \epsilon \\
&= \int_0^\tau (\tau - t) \gamma(v_0) d \left(\rho^2 E[L_{2,T_t}^3] + (1 - \rho^2) E[L_{2,T_t} L_{3,T_t}^2] - \sigma^2 E[T_t L_{2,T_t}] \right) \\
&\quad + \sigma^2 V(T) + \epsilon \\
&= \int_0^\tau (\tau - t) \gamma(v_0) d \left(3\rho^2 \sigma^2 E[T_t L_{2,T_t}] + \rho^2 \kappa_3^L E T_t \right. \\
&\quad \left. + (1 - \rho^2) \sigma^2 E[T_t L_{2,T_t}] - \sigma^2 E[T_t L_{2,T_t}] \right) + \sigma^2 V(T) + \epsilon \\
&= \int_0^\tau (\tau - t) \gamma(v_0) d \left(2\rho^2 \sigma^2 E[T_t L_{2,T_t}] + \rho^2 \kappa_3^L E T_t \right) + \sigma^2 V(T) + \epsilon \\
&= \rho^2 \kappa_3^L O(\tau^2) + (1 + \rho^2) O(\tau^3),
\end{aligned}$$

where ϵ is the error term that has higher order than the previous term. The second equality is due to the stochastic continuity of $\gamma(v_t)$. Thus, Proposition 2 is obtained.

If $\kappa_3^L = 0$, as in the Brownian case, then

$$\text{Cov}(T, L_T^2) = (1 + \rho^2) O(\tau^3)$$

is quadratic in ρ and has the third order of τ . Specifically, we have

$$\lim_{\tau \rightarrow 0} \frac{\text{Cov}(T, L_T^2)}{\tau^3} = \frac{1}{3} \sigma^4 \gamma(v_0)^2 v_0 (1 + \rho^2). \quad (30)$$

For a continuous SVM whose variance v is a diffusion process, the $\text{Cov}(T, L_T^2)$ term converges to 0 according to the argument above. Since

$$\begin{aligned}
E[TB_T] &= E \left[\int_0^\tau v_t dt \int_0^\tau \sqrt{v_t} dW_t \right] \\
&= E \left[\int_0^\tau (\tau - t) \gamma(v_t) dZ_t \cdot \int_0^\tau \sqrt{v_t} dW_t \right] + O(\tau^2) \\
&= \rho E \left[\int_0^\tau (\tau - t) \sqrt{v_t} \gamma(v_t) dt \right] + O(\tau^2) \\
&= \rho C^{xv} + O(\tau^2),
\end{aligned} \quad (31)$$

and the approximation in Proposition 3 is obtained.

Appendix E Proof of Proposition 4

Following the proof of Proposition 2, we first show the order of $\text{Cov}(T, B_T)$. For $T := T_\tau = \int_0^\tau v_t dt$,

$$\begin{aligned}
E[TB_T] &= E \left[\int_0^\tau v_t dt \int_0^\tau \sqrt{v_t} dW_t \right] \\
&= \frac{1}{\Gamma(\alpha)} E \left[\int_0^\tau \left(\int_0^t (t-s)^{\alpha-1} \gamma(v_s) dZ_s \right) dt \cdot \int_0^\tau \sqrt{v_t} dW_t \right] + o(\tau^2) \\
&= \frac{1}{\Gamma(\alpha)} E \left[\int_0^\tau \left(\int_t^\tau (s-t)^{\alpha-1} ds \right) \gamma(v_t) dZ_t \cdot \int_0^\tau \sqrt{v_t} dW_t \right] + o(\tau^2) \\
&= \frac{\rho C^{xv}(\alpha)}{\alpha \Gamma(\alpha)} + o(\tau^2) = O(\tau^{\alpha+1}),
\end{aligned} \tag{32}$$

where $C^{xv}(\alpha) = E \left[\int_0^\tau (\tau-t)^\alpha \gamma(v_t) \sqrt{v_t} dt \right]$. And

$$\begin{aligned}
V(T) &= E \left(\int_0^\tau C_\alpha(\tau-t)^\alpha \gamma(v_t) dW_t \right)^2 + \epsilon \\
&= E \left(\int_0^\tau C_\alpha^2(\tau-t)^{2\alpha} \gamma(v_t)^2 dt \right) + \epsilon \\
&= O(\tau^{2\alpha+1}).
\end{aligned}$$

Next, let $\tilde{B}_T = \int_0^\tau \sqrt{v_s} dZ_s$,

$$\begin{aligned}
\text{Cov}(T, B_T^2) &= E \left[\int_0^\tau (v_t - v_0) dt \cdot (B_T^2 - T + T) \right] + \epsilon \\
&= E \left[\left(\int_0^\tau C_\alpha(\tau-t)^\alpha \frac{\gamma(v_0)}{\sqrt{v_0}} d\tilde{B}_{T_t} \right) (B_{T_\tau}^2 - T) \right] + V(T) + \epsilon \\
&= \int_0^\tau C_\alpha(\tau-t)^\alpha \frac{\gamma(v_0)}{\sqrt{v_0}} d \left(2\rho^2 E \left[T_t \tilde{B}_{T_t} \right] \right) + V(T) + \epsilon \\
&= O(\tau^{2\alpha+1}),
\end{aligned}$$

and the impact of $\text{Cov}(T, B_T^2)$ on ATM skew is of order $O(\tau^{2\alpha-1}) = o(1)$. Hence, we neglect the term and the resulting expression is obtained.

Appendix F Proof of Proposition 5

The term $E[\tilde{T}^2 L_T^2] \leq \sqrt{V(T^2) V(L_T^2)} \leq \sqrt{V(T)^2 V(L_T^2)} = O(\tau^{\frac{7}{2}})$ so the corresponding term in equation (10) converges to 0 as $\tau \rightarrow 0$. This comes from

$V(T^2) = O(\tau^6)$ as a result of the BDG inequality:

$$\begin{aligned}
V(T^2) &= E \left(\int_0^\tau (\tau - t) \gamma(v_0) dL_{T_t} \right)^4 + \epsilon \\
&= E \left(\int_0^\tau t \gamma(v_0) dL_{T_t} \right)^4 + \epsilon \\
&\leq E \left[\sup_{\tau^* \leq \tau} \left(\int_0^{\tau^*} t \gamma(v_0) dL_{T_t} \right)^4 \right] \\
&\leq E \left(\int_0^\tau t^2 \gamma(v_0)^2 dt \right)^2 \\
&= O(\tau^6).
\end{aligned}$$

As we have proved, $\text{Cov}(T, L_T) = O(\tau^2)$ and $\text{Cov}(T, L_T^2) = O(\tau^2)$ in the general jump-diffusion models. And similar to the computation in the proof of Proposition 2, we have

$$\begin{aligned}
\text{Cov}(T, L_T^3) &= E [T(L_T^3 - 3\sigma^2 T L_T - \kappa_3^L T)] + \kappa_3^L V(T) + 3\sigma^2 \text{Cov}(T, T L_T) \\
&= E \left[\left(\int_0^\tau (\tau - t) \gamma(v_0) dL_{2,T_t} \right) \left(\int_0^\tau d(L_{T_t}^3 - 3\sigma^2 T_t L_{T_t} - \kappa_3^L T_t) \right) \right] \\
&\quad + \kappa_3^L V(T) + 3\sigma^2 \text{Cov}(T, T L_T) + \epsilon \\
&= \int_0^\tau (\tau - t) \gamma(v_0) d \left(E[L_{2,T_t}(L_{T_t}^3 - 3\sigma^2 T_t L_{T_t} - \kappa_3^L T_t)] \right) \\
&\quad + \kappa_3^L V(T) + 3\sigma^2 \text{Cov}(T, T L_T) + \epsilon \\
&= \int_0^\tau (\tau - t) \gamma(v_0) d \left(\rho^3 E[L_{2,T_t}^4] + 3\rho(1 - \rho^2)\sigma^2 E[L_{2,T_t}^2 T_t] \right. \\
&\quad \left. - 3\rho\sigma^2 E[T_t L_{2,T_t}^2] - \kappa_3^L E[T_t L_{2,T_t}] \right) + \kappa_3^L V(T) + 3\sigma^2 E T E[T L_T] + \epsilon \\
&= \int_0^\tau (\tau - t) \gamma(v_0) d \left(3\rho^3 \sigma^2 \text{Cov}(T_t, L_{2,T_t}^2 - \sigma^2 T_t) + \kappa_3^L (4\rho^3 - 1) E[T_t L_{2,T_t}] \right. \\
&\quad \left. + \kappa_4^L \rho^3 E[T_t] \right) + \kappa_3^L V(T) + 3\sigma^2 E T E[T L_T] + \epsilon \\
&= \rho^3 \kappa_4^L O(\tau^2) + O(\tau^3),
\end{aligned} \tag{33}$$

where the fourth equation is due to

$$\text{Cov}(T, T L_T) = E T E[T L_T] + E[\tilde{T}^2 L_T] \sim E[T] E[T L_T],$$

and the fifth equation is due to the fourth moment Wald's equation:

$$E[L_{T_t}^4] = 6\sigma^2 E[T_t L_{T_t}^2] + 4\kappa_3^L E[T_t L_{T_t}] + \kappa_4^L E[T_t] - 3\sigma^4 E[T_t^2],$$

with $EL_{T\tau}^4 = O(\tau)$ as long as $\kappa_4^L \neq 0$ and $\rho \neq 0$.

Since we need to compute $\text{Cov}(T, L_T^3) - 3\sigma^2 ETE[TL_T]$ in the equation (14), it happens that the $ETE[TL_T]$ term cancels out. Meanwhile, since $V(T) = O(\tau^3)$ and

$$\text{Cov}(T_t, L_t^2 - \sigma^2 T_t) = O(t^2)$$

by the argument in the proof of Proposition 2. Then $\text{Cov}(T, L_T^3) - 3\sigma^2 ETE[TL_T] = O(\tau^2)$. If $\rho = 0$ but $\kappa_3^L \neq 0$, then $\text{Cov}(T, L_T^3) - 3\sigma^2 ETE[TL_T] = O(\tau^3)$. And Remark 5 follows.

Appendix G Proof of Corollary 2

Under the GJDMs, we have the expression for curvature as

$$\begin{aligned} \text{Cur}(\tau) \approx & \frac{2\gamma_1^L \sigma^3 E[TL_T] + 3\sigma^2 \text{Cov}(T, L_T^2) + 2\bar{\mu}(\text{Cov}(T, L_T^3) - 3\sigma^2 ETE[TL_T])}{6\sigma^5 (ET)^{\frac{5}{2}} \sqrt{\tau}} \\ & - \frac{V(T)}{4\sigma \sqrt{\tau} (ET)^{\frac{5}{2}}} + \frac{\gamma_2^L}{12\sigma (ET)^{\frac{3}{2}} \sqrt{\tau}} - \frac{6\sqrt{\tau}}{\sqrt{ET}} \psi(\tau)^2. \end{aligned}$$

For diffusion models, $\gamma_1^L = \gamma_2^L = 0$, $\text{Cov}(T, B_T^2) = O(\tau^3)$.

Next, we consider the order of $\text{Cov}(T, B_T^3) - 3ETE[TL_T]$. In Brownian cases, we have $\kappa_3^L = \kappa_4^L = 0$ and it has been shown that

$$\text{Cov}(T, B_T^2 - T) = \rho^2 O(\tau^3).$$

Putting into equation (33), we have $\text{Cov}(T, B_T^3) - 3ETE[TL_T] = o(\tau^3)$. Thus, we simplify the formula as

$$\text{Cur}(\tau) \approx \frac{\text{Cov}(T, B_T^2)}{2(ET)^{\frac{5}{2}} \sqrt{\tau}} - \frac{V(T)}{4(ET)^{\frac{5}{2}} \sqrt{\tau}} - \frac{3 \text{Cov}(T, B_T)^2}{2\sqrt{\tau} (ET)^{\frac{7}{2}}}.$$

Its limit form can also be obtained as

$$\begin{aligned} \lim_{\tau \rightarrow 0+} \text{Cur}(\tau) &= \frac{\frac{1}{3}\tau^3 \gamma(v_0)^2 (1 + \rho^2)}{2(v_0 \tau)^{\frac{5}{2}} \sqrt{\tau}} - \frac{\frac{1}{3}\tau^3 \gamma(v_0)^2}{4(v_0 \tau)^{\frac{5}{2}} \sqrt{\tau}} - \frac{3(\frac{1}{2}\tau^2 \rho \gamma(v_0) \sqrt{v_0})^2}{2\tau^4 v_0^{\frac{7}{2}}} \\ &= \frac{\gamma(v_0)^2}{24v_0^{\frac{5}{2}}} (2 - 5\rho^2). \end{aligned}$$

For example, $\gamma(v_t) = \eta \sqrt{v_t}$ and $\sigma = 1$ for Heston models. From (12) and (30),

$$\lim_{\tau \rightarrow 0+} \text{Cur}(\tau) = \frac{1}{24v_0^{\frac{5}{2}}} \eta^2 (2 - 5\rho^2).$$

Appendix H Supplementart Graphs

H.1 2D plots of Term structure for Heston Model

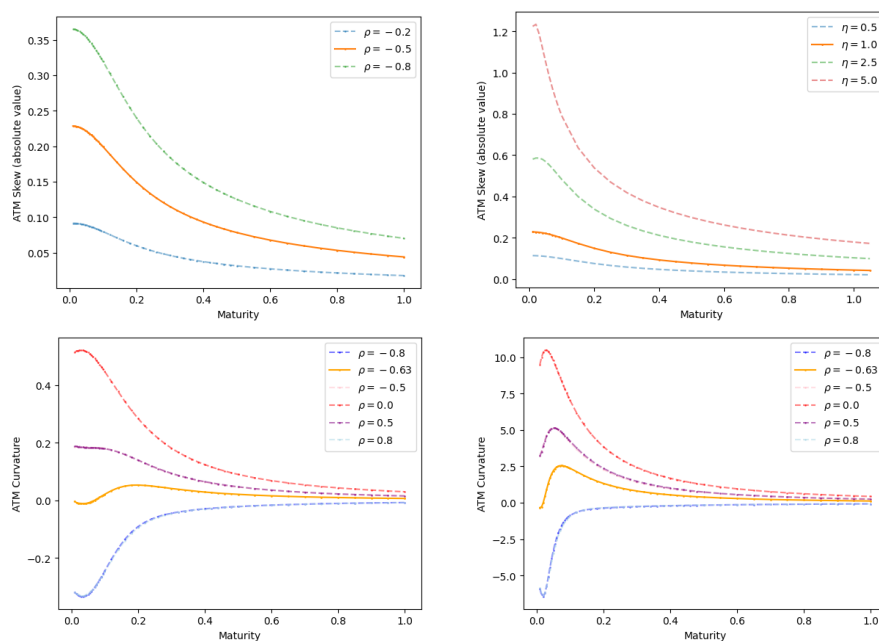


Figure 11: Term structure of ATM volatility skew (first row) and curvature (second row). The same default parameters as in figure (1) is used. The bottom left plot corresponds to vol of vol $\eta = 1$ and the bottom right plot $\eta = 4$. The ATM skew and curvature are plotted for $0.001 \leq \tau \leq 1$.

H.2 Comparison of Two Approximations in Jump models

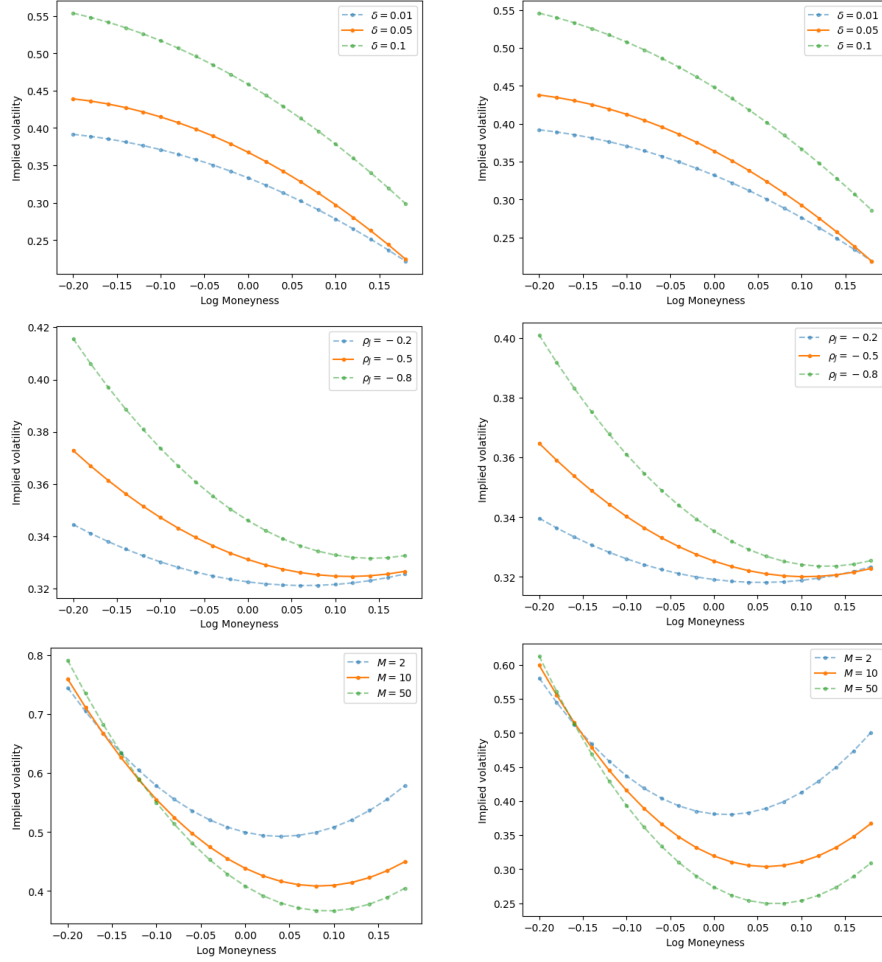


Figure 12: Comparison of approximation (20) (left column) and (4) (right column). Other settings are the same as figure 4.

For the third row, model (2), the approximated quantities are $s = 0.019$, $\gamma_1 = -1.381$, $\gamma_2 = 8.427$ for $M = 10$. And approximation (4) indeed performs better.

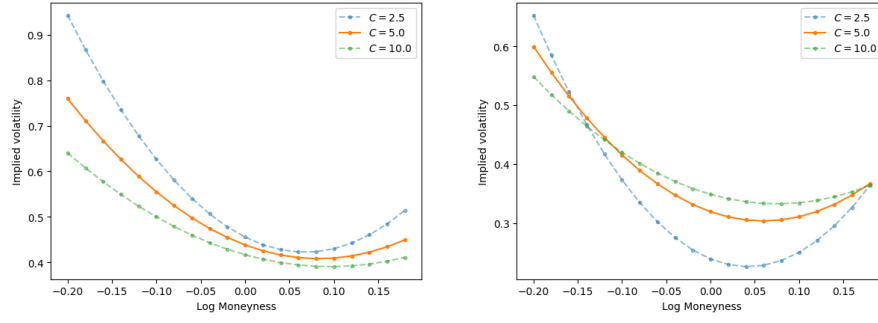


Figure 13: Comparison of approximation (20) (left column) and (4) (right column) for curvature.

Likewise, $\gamma_2 = 8.427$ for $C = 5$ and approximation (4) performs better.